Sea Surface Temperature and Large-Scale Circulation Influences on Tropical Greenhouse Effect and Cloud Radiative Forcing

S. BONY

Laboratoire de Météorologie Dynamique du CNRS, Paris, France

K.-M. LAU AND Y. C. SUD

NASA/Goddard Laboratory for Atmospheres, Greenbelt, Maryland

(Manuscript received 24 April 1996, in final form 13 November 1996)

ABSTRACT

Two independent sets of meteorological reanalyses are used to investigate relationships between the tropical sea surface temperature (SST) and the large-scale vertical motion of the atmosphere for spatial and seasonal variations, as well as for El Niño/La Niña episodes of 1987–88. Supergreenhouse effect (SGE) situations are found to be linked to the occurrence of enhanced large-scale rising motion associated with increasing SST. In regions where the large-scale atmospheric motion is largely decoupled from the local SST due to internal or remote forcings, the SGE occurrence is weak. On seasonal and interannual timescales, such regions are found mainly over equatorial regions of the Indian Ocean and western Pacific, especially for SSTs exceeding 29.5°C. In these regions, the activation of feedback processes that regulate the ocean temperature is thus likely to be more related to the large-scale remote processes, such as those that govern the monsoon circulations and the low-frequency variability of the atmosphere, than to the local SST change.

The relationships among SST, clouds, and cloud radiative forcing inferred from satellite observations are also investigated. In large-scale subsidence regimes, regardless of the SST range, the cloudiness, the cloud optical thickness, and the shortwave cloud forcing decrease with increasing SST. In convective regions maintained by the large-scale circulation, the strong dependence of both the longwave (LW) and shortwave (SW) cloud forcing on SST mainly results from changes in the large-scale vertical motion accompanying the SST changes. Indeed, for a given large-scale rising motion, the cloud optical thickness decreases with SST, and the SW cloud forcing remains essentially unaffected by SST changes. However, the LW cloud forcing still increases with SST because the detrainment height of deep convection, and thus the cloud-top altitude, tend to increase with SST. The dependence of the net cloud radiative forcing on SST may thus provide a larger positive climate feedback when the ocean warming is associated with weak large-scale circulation changes than during seasonal or El Niño variations.

1. Introduction

Water vapor and clouds are the main modulators of the earth radiation budget (Houghton 1990). In case of a naturally or anthropogenically produced beginning of climate warming, their dependence on surface temperature and the way they affect radiation fluxes at the top of the atmosphere can thus be the primary drivers of huge climate feedbacks. To investigate the sign of these feedbacks, many observational studies have investigated relationships between spatial or short-term temporal variations of the SST and the water vapor greenhouse effect and cloud radiative forcing. For example, positive correlations between SST, water vapor, and clear-sky greenhouse effect have been interpreted as a manifestation of the positive water vapor feedback (Raval and Ramanathan 1989; Stephens and Greenwald 1991a). Subsequently, Stephens and Greenwald (1991b) investigated the impact of clouds on the greenhouse effect, and Ramanathan and Collins (1991) analyzed relationships between SST and cloud radiative forcing anomalies during the 1987 El Niño to propose a regulatory mechanism of the tropical SST involving interactions among SST, deep convection, and highly reflective cirrus clouds.

While water vapor and clouds are affected by local SST changes through the activation of thermodynamical processes within the atmospheric column, they are sensitive to many other factors that may depend only partly on the local SST. Among those factors is the large-scale atmospheric circulation, which transports heat and moisture and affects the thermodynamical stability of the atmosphere on large spatial scales. On short timescales, SST variations are very inhomogeneously distributed

Corresponding author address: Dr. Sandrine Bony, Laboratoire de Météorologie Dynamique du CNRS, Ecole Normale Supérieure, 24 rue Lhomond, 75231 Paris Cedex 05, France.
E-mail: bony@lmd.ens.fr

over the tropical ocean and are thus associated with profound modifications of the large-scale atmospheric circulation. The dependence of water vapor and clouds on SST thus partly stems from large-scale dynamical influences. According to the type of climate variations and the timescale under consideration, a given SST change may be accompanied by vastly different changes of the large-scale circulation. For example, the perturbations of the atmospheric circulation may be smaller for weak and long-term climate changes than for seasonal or short-term interannual variations. A given SST change may thus be associated also with vastly different changes of water vapor and clouds. To determine whether the relationships inferred from the short-term variability may be extrapolated to longer-term climate changes or used to assess model feedbacks operating in climate change experiments, one has thus to estimate the dynamical dependence of relationships between the SST and water vapor, clouds, and radiation. This provides the main motivation for conducting the present study.

Though the importance of the large-scale atmospheric convergence in driving the observed correlations between SST, atmospheric greenhouse effect, and cloudiness has been pointed out by Ramanathan and Collins (1991), the role of large-scale dynamical influences in influencing water vapor, clouds, and radiation has drawn considerable attention during the past few years. For instance, Hallberg and Inamdar (1993) and Weaver et al. (1994) show that the occurrence of ''supergreenhouse'' situations (which correspond to cases where the increase of the greenhouse effect with surface temperature is larger than that of the surface infrared emission) cannot be explained by thermodynamical feedback processes only. They suggest that large-scale dynamical processes are involved. The actual contribution of thermodynamical processes to water vapor and clear-sky greenhouse effect changes is investigated by Bony et al. (1995a): less than 30% for seasonal or El Niño/La Niña variations against more than 80% for long-term climate change experiments. The influence of the large-scale atmospheric dynamics on the cloud radiative forcing has been stressed also by many studies. Fu et al. (1992) show, by comparing western and eastern regions of the tropical pacific between El Niño and non–El Niño April months, that the radiative effects of cirrus clouds are more controlled by changes in large-scale atmospheric circulation than directly by SSTs. The influence of large-scale dynamical influences on cloud and radiation fields is also pointed out by Hartmann and Michelsen (1993), who show the strong correspondence between the spatial distribution of the shortwave cloud radiative forcing and that of the large-scale vertical motion for the March–May season during 1987. Waliser et al. (1993) show that despite their very high SST (higher than 29.5°C), ''hot spots'' of the tropical ocean are generally associated with diminished convection. Waliser (1996) shows the important role that remotely forced atmospheric variability plays in suppressing deep convection over these regions. Finally, Lau et al. (1994) show by using a cumulus ensemble model that over the warm pool, remotely forced vertical motion changes can have a stronger control on the variation of cloud radiative forcing and greenhouse effect than local SST. Based on Lindzen and Nigam's (1987) study, Lau et al. (1994) argue that the SST gradient is more important than local SST in determining the large-scale vertical motion. However, Ramanathan et al. (1994) replies that SST and large-scale vertical motion are not independent from each other. They argue in particular that a local increase in warm ocean SST enhances the SST gradient and thus promotes the large-scale convergence into the region of warming. Evidently, there is a considerable debate on the issue of the relative influence of local SST versus remote effects on the large-scale vertical motion of the atmosphere. This reinforces our motivation for conducting the present study.

By using recent meteorological reanalyses produced by using frozen state-of-the-art versions of the global data assimilation system (GDAS), we investigate how the SST and the large-scale atmospheric vertical motion are related for spatial, seasonal, and El Niño/La Niña variations during 1987–88 over tropical ocean (30°S–30°N). Then, by using additional satellite data of water vapor, clouds, and radiation, we investigate and quantify the influence of large-scale circulation changes on the occurrence of supergreenhouse effect situations, and on the dependence of the cloud radiative forcing on SST.

Satellite data and meteorological reanalyses are presented in section 2. In section 3, we show how spatiotemporal relationships between SST and water vapor and cloud and radiation parameters depend on the large-scale vertical motion of the atmosphere. In section 4, we characterize locally the relationship between the variability of the SST and that of the vertical motion during seasonal and El Niño/La Niña variations. Regions where remote effects are important are outlined. Then, in section 5, we investigate the dependence of the supergreenhouse effect and of the cloud radiative forcing on SST and large-scale circulation influences. A summary and a discussion are reported in section 6.

2. Data and meteorological reanalyses

All satellite data used in this study are monthly means for the period January 1987 to December 1988 and are used at the resolution 2.5° × 2.5°. Radiative fluxes at the top of the atmosphere for clear-sky and cloudy conditions are derived from the Earth Radiation Budget Experiment (ERBE; Barkstrom 1984). Cloud fraction, cloud water path, and cloud optical thickness data are derived from the International Satellite Cloud Climatology Project (ISCCP) C2 dataset (Rossow et al. 1991; Rossow and Schiffer 1991); monthly mean sea surface temperatures are derived from the improved data analysis produced at the National Centers for Environmental

Prediction (NCEP) (Reynolds and Smith 1994). These data are available from the National Aeronautics and Space Administration (NASA) on the GEWEX–ISLSCP CD-ROMs (Meeson et al. 1995; Sellers et al. 1995). We also used upper relative humidity and cloud fraction data derived from the Tiros Operational Vertical Sounder (TOVS) Pathfinder Path A dataset produced at the Goddard Laboratory for Atmospheres (Susskind et al. 1996).

We used reanalyses of the global atmosphere for the period 1987–88 produced independently at the Data Assimilation Office (DAO) of the Goddard Laboratory for Atmospheres (Schubert et al. 1993) and at NCEP (Kalnay et al. 1996). These two sets of reanalyses were produced by assimilating all available recorded observations into a frozen state-of-the-art global data assimilation system developed independently at the two centers. In this study, DAO and NCEP–NCAR monthly mean reanalyses are used at a resolution of 2.5° × 2.5°.

The comparison, as well as the assessment vis-à-vis satellite data, of the atmospheric hydrological and radiative fields derived from the two reanalyses are presented in a companion paper (Bony et al. 1997). Dynamical fields are the only fields of the reanalyses that are considered in this study. They are used to investigate the effects of the large-scale atmospheric circulation on the satellite observed greenhouse effect and cloud radiative forcing. As a first step, it is thus important to ensure that the large-scale dynamical features described by the reanalyses are consistent with the satellite observed features of the atmosphere. Prabhakara et al. (1979), followed by Stephens (1990), proposed to highlight the effects of large-scale motion on atmospheric water vapor through the parameter $(W - \overline{W})/W$, where W is the regional monthly mean precipitable water and $\overline{W}$ the value estimated given the SST and the mean relationship between the SST and the columnar water. Regions influenced by moisture convergence are characterized by positive values of this parameter, and regions influenced by moisture divergence are characterized by negative values (Stephens 1990). This parameter is also a gross indicator of the depth of the maritime boundary layer (Prabhakara et al. 1979) and of the vertical structure of the atmosphere (Bony and Duvel 1994). This parameter is used here as a way of quantifying the effects of large-scale circulation on precipitable water both in the reanalyses and in satellite observations. A fairly good agreement is found between Special Sensor Microwave/Imager (SSM/I) data, TOVS data, NCEP reanalyses, and DAO reanalyses when considering either the spatial distribution of the frequency of occurrence of large-scale moisture convergence [positive $(W - \overline{W})/W$ values] for the period July 1987–December 1988 (Fig. 1a) or this frequency binned into SST intervals of 1 K (Fig. 1b). Differences between reanalyses and satellite data being of the same order as differences between SSM/I and TOVS data, the large-scale atmospheric motions depicted by the reanalyses are consistent with satellite observations. This makes it possible to use jointly these different datasets.

3. Spatiotemporal relationships

a. Observed relationships between SST, clouds, and radiation

Spatiotemporal relationships between the SST and water vapor and cloud or radiation parameters derived from independent satellite datasets during 1987–88 over tropical ocean (30°S–30°N) exhibit common characteristic features: a large standard deviation around the SST-binned atmospheric variables and two discontinuities in the slope of the relationships for SSTs of about 26°–27°C and 29.5°C (Fig. 2).

For example, the clear-sky outgoing longwave (LW) flux LW_{clear} globally increases with SST for SSTs smaller than 26°–27°C (Fig. 2a). This increase with temperature of the atmospheric infrared emission toward space constitutes a fundamental thermal regulating process of the atmosphere–ocean climate system. For 26°–27°C ≤ SST ≤ 29.5°C, however, LW_{clear} decreases with increasing SST. This behavior is commonly referred to as clear-sky supergreenhouse effect situations (Ramanathan and Collins 1991). It corresponds to cases when the increase with SST of the infrared absorption by water vapor exceeds the increase of the surface and atmospheric infrared emission with temperature. In these situations, the ocean–atmosphere system loses its fundamental regulating process associated with the coupling between temperature and thermal radiation. This strong water vapor greenhouse effect is closely related to enhanced tropospheric humidity in the upper troposphere (Fig. 2b), which absorbs and reemits LW radiation at very low temperatures. For SSTs above about 29.5°C, the sign of the LW_{clear}-SST slope changes and becomes positive. Consistently, the upper-tropospheric humidity decreases slightly.

Similar relationships are found for cloud parameters. The SW and LW components of the cloud radiative forcing (C_{SW} and C_{LW}) originally defined by Coakley and Baldwin (1984) primarily depend, respectively, on the cloud albedo and on the cloud-top temperature (which is closely related to the cloud-top altitude). We note, indeed, a strong coherence between C_{LW} and the cloud-top pressure (Figs. 2c,d), and between C_{SW} and the cloud optical thickness (Figs. 2e,f). The slope of the mean relationship with SST of each of these variables exhibit clearly the two discontinuities previously noticed at 26°–27°C and 29.5°C.

b. Relationship between the SST and the large-scale vertical motion

To investigate the role of large-scale dynamical influences in these discontinuities, we analyze the dynamical fields that are derived from the two independent

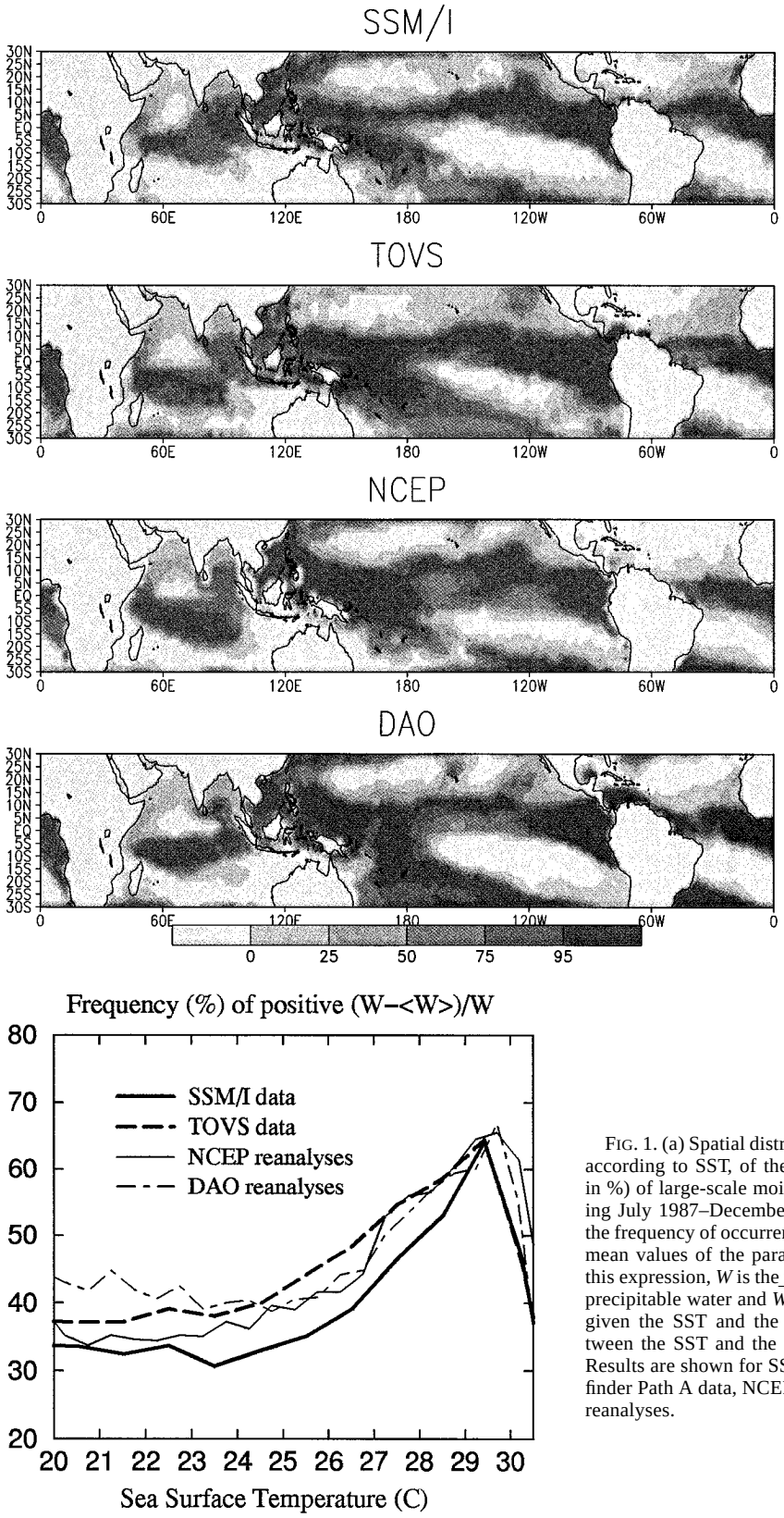

FIG. 1. (a) Spatial distribution and (b) binning according to SST, of the frequency (expressed in %) of large-scale moisture convergence during July 1987–December 1988, as depicted by the frequency of occurrence of positive monthly mean values of the parameter $(W - \overline{W})/\overline{W}$. In this expression, W is the regional monthly mean precipitable water and $\overline{W}$ is the value estimated given the SST and the mean relationship between the SST and the columnar water vapor. Results are shown for SSM/I data, TOVS Pathfinder Path A data, NCEP reanalyses, and DAO reanalyses.

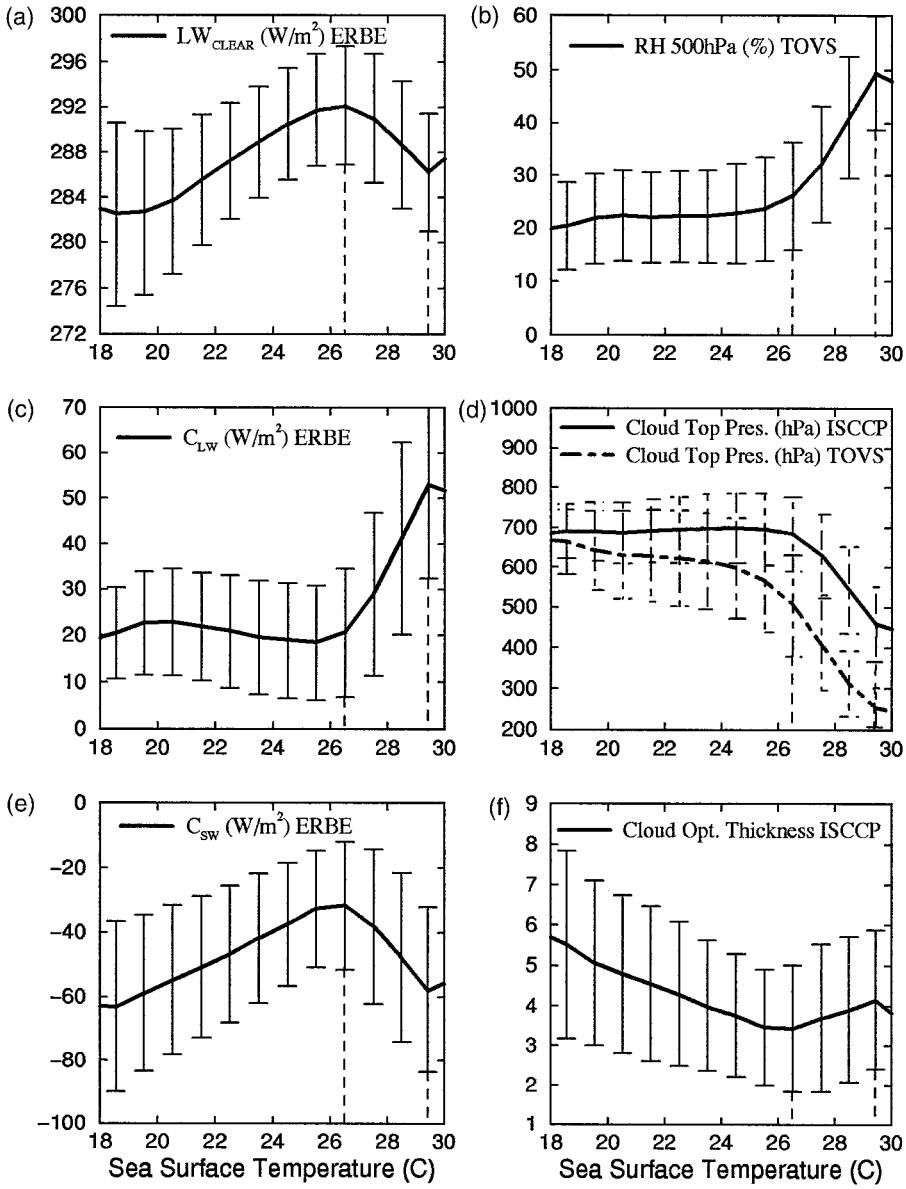

FIG. 2. Mean relationships between the SST and the (a) clear-sky outgoing LW flux derived from Earth Radiation Budget Experiment (ERBE) data, (b) upper relative humidity derived from TOVS data, (c) LW cloud radiative forcing derived from ERBE data, (d) cloud-top pressure derived from ISCCP and TOVS data, (e) SW cloud radiative forcing derived from ERBE data, and (f) cloud optical thickness derived from ISCCP data. All relationships are based on 2.5° × 2.5° monthly means data during 1987–88 over tropical ocean (30°S–30°N). Vertical bars represent ± the standard deviation around the 1987–88 mean. The three SST regimes discussed in the text are highlighted by dotted vertical lines.

sets of meteorological reanalyses produced at DAO and at NCEP (section 2).

The vertical velocity at 500 hPa is a good proxy of the large-scale vertical motion associated with the large-scale tropical circulation (the divergence at 200 hPa is another equivalent proxy, since it is closely related to the vertical velocity at 500 hPa through the mass balance requirements). As shown in Fig. 3, the occurrence of large-scale rising motion situations (negative 2.5° × 2.5° monthly mean vertical velocities $\omega = dp/dt$; sinking motions correspond to positive monthly mean values of ω) is a strong function of SST and exhibits the same discontinuities as those seen in Fig. 2. For tropical SSTs less than about 26°–27°C, less than 20% of regional monthly means are characterized by large-scale rising motion. Mostly subsiding motions are thus found over the tropical oceans for this range of SST. This favors the occurrence of the low-level cloudiness over these

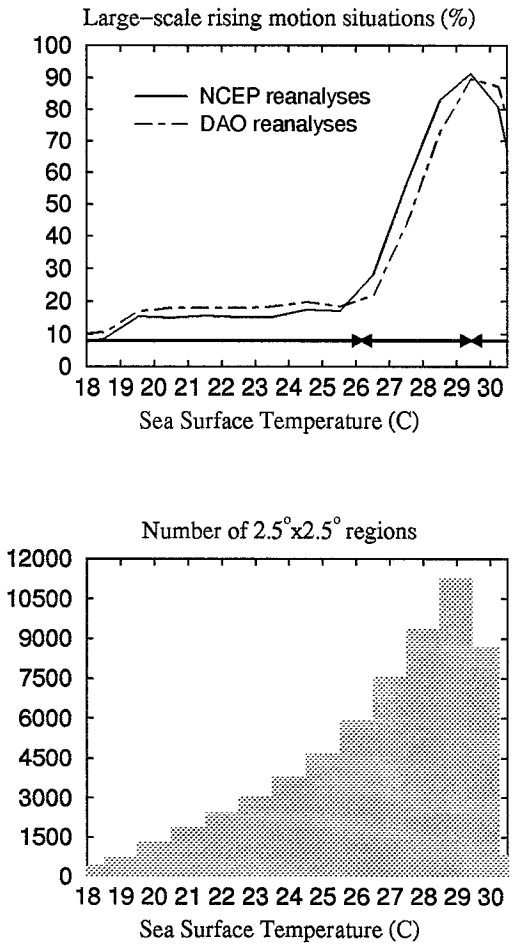

FIG. 3. (a) For NCEP and DAO reanalyses, percentage of large-scale rising motion situations (negative monthly mean value of the 500-hPa vertical velocity $\omega = dp/dt$) for each SST interval of 1 K over tropical ocean (30°S–30°N) during 1987–88. The three SST regimes discussed in the text are highlighted at the bottom of the figure. (b) Number of 2.5° × 2.5° regions associated with each SST interval.

regions (Fig. 2d). The percentage of large-scale rising motion increases sharply as the SST reaches 26°–27°C, up to reaching about 90% at 29.5°C. Above 29.5°C, the percentage of large-scale subsidence situations increases, and the proportion of large-scale rising motions decreases accordingly. As suggested by Waliser and Graham (1993), this large-scale subsidence may be forced by nearby or remotely generated deep convection. The remarkable agreement between the two sets of reanalyses shows that these results are not dependent on the global assimilation system used to produce the reanalyses [in particular, DAO and NCEP use different general circulation models using different convection schemes (cf. Bony et al. 1997)]. The three SST regimes found in Fig. 2 thus correspond to three different relationships between the SST and the large-scale vertical motion of the atmosphere.

We define different regimes of the large-scale atmospheric motion (Table 1; Bony et al. 1995b) ranging from strong rising motion (large negative monthly mean values of ω, so-called regime 1) to strong subsidence motion (regime 6). We consider regular intervals of 20 hPa day^{-1}, except for subsidence regimes where the range of variation of ω is narrower. Again, the percentage of occurrence of each of these six regimes is quite similar for DAO and NCEP reanalyses. Figure 4

TABLE 1. Definition of the large-scale circulation regimes as a function of the monthly mean vertical velocity ω. Also reported is the occurrence of each regime in DAO and NCEP reanalyses, expressed as a percentage of the total number of situations (61 645 pixels of 2.5° × 2.5°) during 1987–88 over tropical ocean (30°S–30°N).

Regime	ω range (hPa day^{-1})	Occurrence DAO	Occurrence NCEP
1	$\omega < -40$	10%	10%
2	$-40 < \omega < -20$	12%	16%
3	$-20 < \omega < 0$	22%	22%
4	$0 < \omega < 20$	31%	25%
5	$20 < \omega < 30$	15%	14%
6	$30 < \omega$	10%	13%

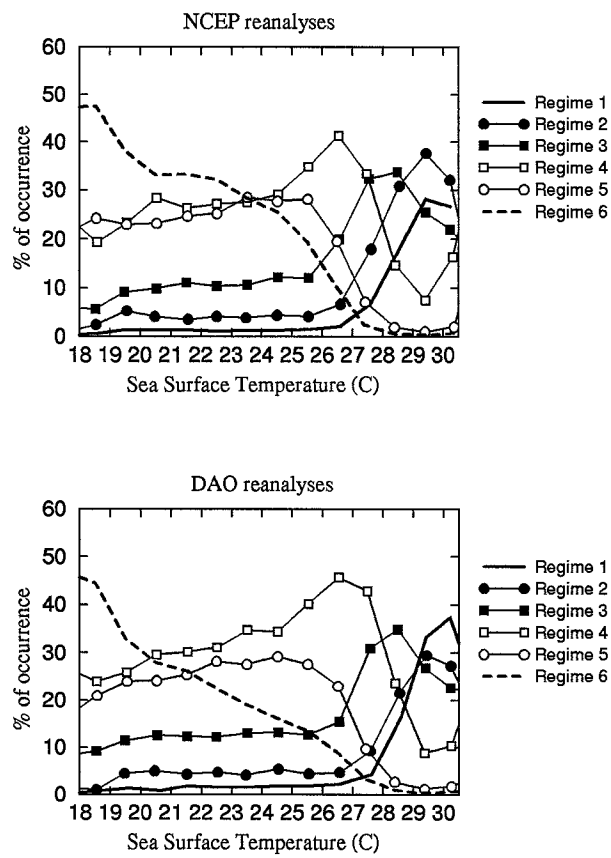

FIG. 4. For each SST interval of 1 K, percentage of occurrence of the different large-scale circulation regimes defined in Table 1 over tropical ocean during 1987–88 for (a) NCEP reanalyses and (b) DAO reanalyses.

presents the probability of occurrence of these six large-scale circulation regimes as a function of the SST (the sum of regimes 1, 2, and 3 gives the percentage of large-scale rising motions reported on Fig. 3). It shows that a given value of the SST can be associated with a wide range of large-scale vertical motions, in particular within the range 26°–28°C. The thermodynamic local influence of the SST on the overlaying vertical motion is thus strongly modulated by other factors. Among those factors is the influence of remote SST changes on the large-scale temperature gradients, which are a forcing of the low-level atmospheric convergence (Lindzen and Nigam 1987). The definition of these different dynamical regimes, and their binning according to SST, is a convenient way of unraveling the SST–greenhouse effect relationships in terms of large-scale circulation influences. It should be emphasized, however, that these regimes are somewhat coupled with each other through the general circulation of the atmosphere as well as mesoscale circulations. This is especially true over warm regions of the tropical oceans, where regions of large-scale subsidence are likely to be forced by nearby or remotely generated rising motions.

The probability of occurrence of the different large-scale circulation regimes varies with the SST (Fig. 4). As expected, we find that the occurrence of strong subsidence (regime 6) strongly decreases as the SST increases. Those situations are found mainly over the eastern side of the ocean basins cooled by an oceanic upwelling (not shown). For SSTs less than about 26°C, the relative occurrence of the different circulation regimes does not depend much on the SST. For warmer SSTs on the contrary, both the frequency and the intensity of large-scale rising motions increase with the SST. The apparent ''threshold'' value of the SST above which this increase starts ranges from 26°C for regime 3 to 27.5°C for regime 1. For SSTs above 29.5°C, very strong rising motions are still frequent, but the occurrence of weak subsidence increases.

The relationships between the large-scale rising motion and the SST over warm oceans are very consistent with those inferred between the tropical deep convection and the SST in previous observational studies. In these studies, radiative quantities were chosen as proxies for the convection [usually the outgoing longwave radiation (OLR), convective cloudiness, or high reflective cirrus clouds]. For example, Gadgil et al. (1984) and Graham and Barnett (1987) pointed out the sharp increase of deep convection for SSTs above 26°–27°C. Waliser et al. (1993) showed that regions of SST larger than 29.5°C are generally associated with diminished convection. Zhang (1993) showed that over the warm pool, deep convection becomes more frequent and, when it occurs, tends to be more intense. As suggested by Hartmann and Michelsen (1993), the 2.5° × 2.5° large-scale rising motion over warm regions is thus intrinsically related to the occurrence and the intensity of tropical deep convection over the 2.5° × 2.5° domain. Indeed, the large-scale atmospheric motions force the tropical convection through their transports of heat and moisture in the lower levels of the atmosphere and by influencing the large-scale stability of the atmosphere (Fu et al. 1996). In return, the tropical convection contributes to the large-scale atmospheric motions through its impact on the latent heat release and the radiation cooling and then on the atmospheric temperature profile (Emanuel et al. 1994).

c. *Circulation-stratified relationships*

1) RELATIONSHIP BETWEEN SST AND CLEAR-SKY OLR

To investigate large-scale dynamical influences on the LW_{clear}–SST relationship presented in Fig. 2, we stratify these relationships into the different circulation regimes defined in Table 1. Results obtained by using either NCEP or DAO reanalyses to classify the tropical regions into the different dynamical regimes are very similar (Figs. 5a,b). This gives confidence in using this large-scale flow classification to analyze the variability of the satellite-derived LW_{clear}. In large-scale subsidence regimes (regimes 4, 5, 6), LW_{clear} increases with the SST over the whole range of tropical SSTs and supergreenhouse effect situations do not occur. In these regions, the low-level humidity increases with the SST (not shown). However, the increase of the thermal emission of the surface and the atmosphere with temperature exceeds that of the water vapor infrared absorption. Note that for SSTs larger than about 27°C, the upper relative humidity of subsidence regions increases slightly with SST. This is likely to reflect the moistening effect of the moist air diverging from the top of the surrounding convective towers toward the upper troposphere of subsiding regions. In large-scale rising motion regimes (regimes 1, 2, 3), LW_{clear} is systematically smaller than in sinking regimes. This is because the organization of deep convection in large-scale rising motions is accompanied by a moistening of the upper troposphere (Fig. 6), which enhances the greenhouse effect. Note that the large standard deviation associated with the mean LW_{clear}–SST relationship (Fig. 2) is well explained by the large-scale circulation variability for a given range of SST.

For individual large-scale circulation regimes, the slopes of LW_{clear}–SST relationships are positive or only weakly negative, and the two SST discontinuities noticed on the mean LW_{clear}–SST are strongly attenuated (Fig. 5). This confirms the role of large-scale dynamical influences in these discontinuities. This shows in particular that the apparent discontinuity at 26°–27°C results from the increase of both the frequency and the intensity of large-scale rising motions with SST (Fig. 4), which gives a larger statistical weight to regimes 4, 5, 6 as the SST increases. The discontinuity at 29.5°C is due to a larger statistical weight of regime 4.

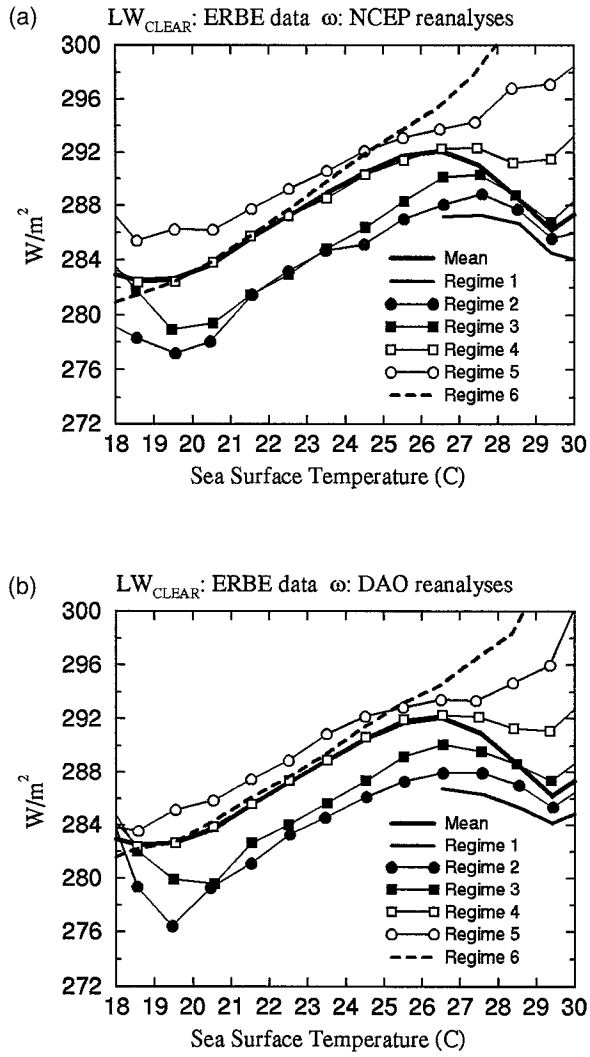

FIG. 5. Mean and circulation-stratified relationships between the clear-sky LW flux at the top of the atmosphere (ERBE data) and the SST (Reynolds data). The different regimes of large-scale circulation correspond to different ranges of monthly mean vertical velocity at 500 hPa ω derived from (a) NCEP reanalyses and (b) DAO reanalyses.

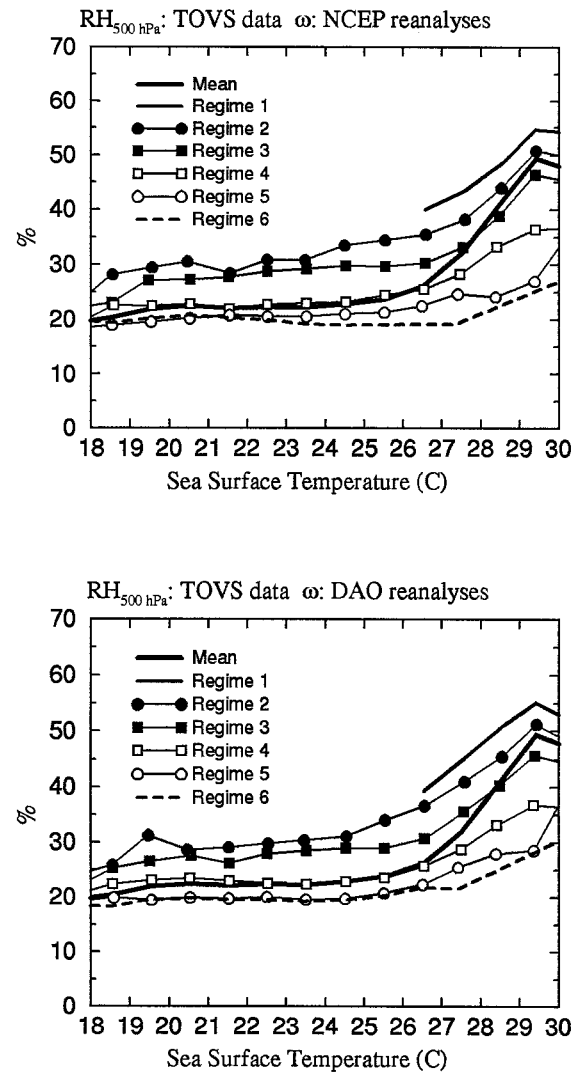

FIG. 6. Same as Fig. 5 except for the relative humidity at 500 hPa derived from TOVS data.

2) RELATIONSHIPS BETWEEN SST AND CLOUD RADIATIVE FORCING

Similar analyses are done for the cloud radiative forcing and associated cloud parameters derived from independent satellite datasets (Fig. 7). Note that for the cloud fraction, ISCCP and TOVS data are substantially different. This is due to different definitions of the cloud amount (in contrast with ISCCP data, TOVS algorithms give effective cloud amounts, i.e., the cloud fraction times the cloud longwave emissivity) and also to different algorithms used to determine whether an observed scene is clear or cloudy (J. Susskind 1995, personal communication). Since results obtained by using NCEP and DAO reanalyses for the definition of the large-scale circulation regimes are very similar (Figs. 5 and 6), we present hereafter results obtained by using DAO reanalyses only.

The relationships between the LW and SW cloud forcing and the SST highly depend on the large-scale circulation regime under consideration (Fig. 7). In large-scale subsidence regimes, mainly associated with low-level stratiform clouds (Fig. 7d), C_{LW} only weakly decreases while C_{SW} is strongly negatively correlated with the SST. This is related in part to the decrease of the cloud optical thickness with SST (Fig. 7c). Since the atmospheric temperature is positively correlated to the SST, this indicates also the decrease of the cloud optical thickness with cloud temperature in large-scale subsidence regimes. This is in accordance with findings of Tselioudis et al. (1992). We note also a decrease of the low-level cloud fraction (Figs. 7e,f) over a very large range of tropical SSTs. These findings confirm and ex-

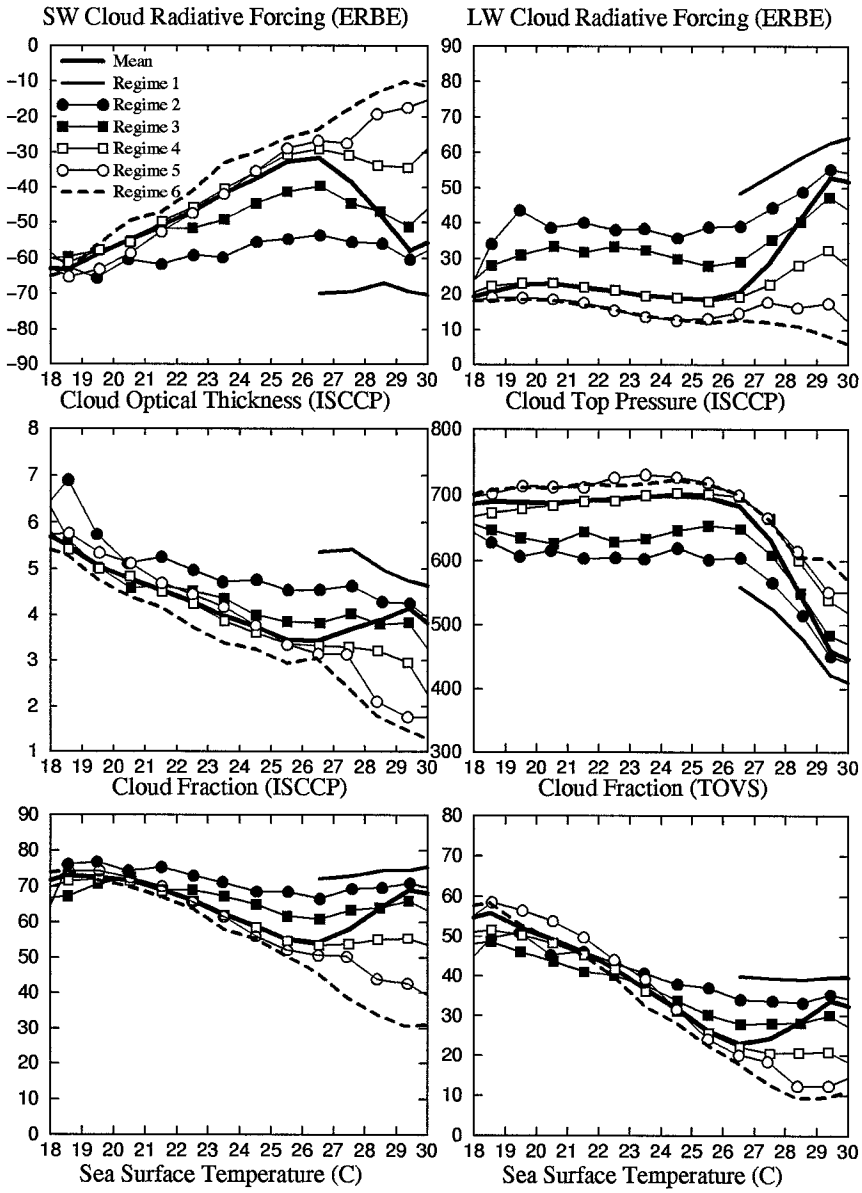

FIG. 7. Mean and circulation-stratified relationships between the SST and the (a) SW cloud radiative forcing, (b) LW cloud radiative forcing, (c) cloud optical thickness, (d) cloud-top pressure, (e) cloud fraction derived from ISCCP data, and (f) cloud fraction derived from TOVS data. The different large-scale circulation regimes are defined from DAO reanalyses.

tend observational results of Oreopoulos and Davies (1993) and Norris and Leovy (1994) derived over cold ocean regions as well as numerical process studies (Albrecht 1981; Betts and Ridgway 1989). It is not clear, so far, whether this anticorrelation is due mostly to the cooling of the SST by the solar screening of low-level clouds or rather to the sensitivity of clouds themselves to the local SST through a modification in the boundary layer properties.

In large-scale rising motion regimes of the middle troposphere, on the contrary, the dependence of C_{SW} on SST is weak (Fig. 7a). This is consistent with the weak variation of the cloud amount with SST (Figs. 7e,f) and the decrease of the cloud optical thickness (Fig. 7c) that are inferred from independent datasets. The decrease of the cloud optical thickness with SST is primarily due to the decrease of the cloud water path (not shown) despite the higher elevation of clouds (Fig. 7d). The increase of the precipitation with SST for a given large-scale circulation regime (not shown) may thus explain the decrease of the cloud water path. The mean relationships between SST and C_{SW} and the cloud optical thickness and the cloud fraction is thus more related to large-scale vertical motion changes (which give a larger

statistical weight to large-scale convergence regimes as the SST increases) than to thermal SST effects. Moreover, the large dispersion of C_{SW} values for a given SST (more than 60 W m^{-2} over warm regions) is well explained by the variability of the large-scale vertical motion for a given SST (Fig. 7a). Over colder regions, on the other hand, the large standard deviation appearing around the mean SST–C_{SW} relationship (Fig. 2a) is not well explained by the variability of the large-scale circulation. Other factors must then be invoked, such as the variability of the incoming solar radiation, the surface wind speed, the horizontal gradients of humidity, and the microphysical properties of stratiform clouds, including the liquid water distribution within the cloud layer (e.g., Cahalan et al. 1994; Klein et al. 1995).

Finally, the dependence of C_{LW} on SST for a given large-scale convective regime is larger than that of C_{SW} (Fig. 7a). As will be explained later (section 5b), this may be due to the thermodynamical sensitivity of the cloud-top height to SST changes (Fig. 7d).

4. Local relationships between SST and large-scale vertical motion

The above analysis of spatiotemporal relationships (section 3) shows that the change of water vapor, clouds, or radiation with SST strongly depends on large-scale vertical motion changes that generally accompany SST variations. It also shows that, on the basis of spatiotemporal relationships, both the frequency and the intensity of large-scale rising motions increase with increasing SST. We investigate below the space and timescales on which this behavior holds. We examine in particular the validity of these statistical relationships at single locations of the tropical ocean by investigating *locally* the relationships between seasonal and El Niño/La Niña changes of the SST and of the large-scale vertical motion.

a. Characterization of SST-vertical motion changes

At each grid point, we compute seasonal anomalies of SST and large-scale vertical motion by subtracting the 1987 (respectively, 1988) annual average from 1987 (1988) monthly means. El Niño/La Niña anomalies are computed in each grid point by subtracting 1987 and 1988 monthly means for each month. We classify the relative changes of the SST and of the large-scale vertical motion into three categories, which characterize both the relative sign of SST and ω changes and the magnitude of the ω change normalized by the SST change:

case I: $\Delta\omega/\Delta\mathrm{SST} < -10$ hPa day^{-1} K^{-1}

case II: $\Delta\omega/\Delta\mathrm{SST} > +10$ hPa day^{-1} K^{-1}

case III: $-10 < \Delta\omega/\Delta\mathrm{SST} < +10$ hPa day^{-1} K^{-1}.

To avoid infinite values of the ratio $\Delta\omega/\Delta\mathrm{SST}$, we disregard seasonal or interannual changes for which $|\Delta\mathrm{SST}| \leq 0.01$ K. The value of this threshold is not critical for our results. The first category (case I) corresponds to the simultaneous increase (or the simultaneous decrease) of the SST and of the large-scale upward motion. Here, ω changes can be due to the local influence of the SST on the moist static energy of the planetary boundary layer and thus on the occurrence of deep convection on large spatial scales. They can also be driven by remote forcings independent on the local SST change. Case II corresponds to the simultaneous increase of the SST and of the large-scale subsidence (or the simultaneous decrease of the SST and increase of the large-scale rising motion). In that case, the change in the intensity of the large-scale motion cannot be explained by any local SST influence and is rather related to remote forcings. Among examples of remote influences that may inhibit the large-scale rising motion of the atmosphere as the SST increases is the occurrence of a large-scale subsidence induced by surrounding ascending regions or the suppression of the onset of deep convection through the drying of the planetary boundary layer by large-scale moisture transports (Fu et al. 1994). The third category (case III) refers to situations for which SST changes are accompanied by weak or no vertical motion changes.

TABLE 2. Definition of the three categories (hereafter referred to as case I, case II, case III) of SST–large-scale vertical motion relationships for seasonal and El Niño/La Niña variations during 1987–88. The occurrence of each case for DAO and NCEP reanalyses over the whole tropical ocean is reported and expressed as a percentage of the maximum possible occurrence: 61 920 for seasonal variations, 30 778 for El Niño/La Niña variations.

	Seasonal		El Niño/ La Niña	
	DAO	NCEP	DAO	NCEP
Case I: $\Delta\omega/\Delta SST < -10$ hPa day^{-1} K^{-1}	40%	40%	44%	47%
Case II: $\Delta\omega/\Delta SST > +10$ hPa day^{-1} K^{-1}	17%	19%	29%	28%
Case III: $\lvert\Delta\omega/\Delta SST\rvert \leq 10$ hPa day^{-1} K^{-1}	43%	41%	27%	25%

The occurrence of these three categories over the whole tropical ocean during 1987–88 is reported in Table 2 for DAO and NCEP reanalyses. Figure 8 presents their spatial distribution for NCEP reanalyses (DAO reanalyses give similar results), and Figure 9 presents their occurrence binned into SST intervals of 1K. For seasonal variations, SST intervals are defined from the annually averaged SST. They are defined from the 1988 monthly mean SST for El Niño/La Niña variations. Results are very similar for NCEP and DAO assimilation products, showing that they produce similar seasonal and interannual changes of the large-scale circulation.

b. Seasonal variations

For seasonal variations, cases I and III are the most populated (Table 2), each of them representing about 40% of the total number of regional seasonal variations (about 61900). Case III dominates over subtropical ocean regions poleward of about 20° of latitude and on the eastern side of ocean basins (Fig. 8), for SSTs less than about 24°–25°C (Fig. 9). In these regions, where large-scale subsidence situations prevail, the variability of the large-scale vertical motion is largely independent from that of local SST changes.

Regions where the vertical motion changes are the most correlated to local SST changes (case I) mainly occur around 10°–20° of latitude (Fig. 8). At these latitudes, the seasonal migration of the ascending and descending branches of the Hadley circulation has a large influence on regional vertical motion changes. Moreover, these regions are mainly located on the 27°–28°C isotherm (Fig. 9). Betts and Ridgway (1989) showed that when the SST exceeds about 27°C, the moist enthalpy of the planetary boundary layer is sufficient to give deep convective instability and to promote the development of organized deep convection. Large-scale vertical motion changes in these regions are thus likely to result from a cooperation of large-scale dynamical influences associated with the Hadley circulation and thermodynamical influences related to local SST changes.

Case II situations occur when the atmospheric vertical motion is not related to the local SST—that is, when the subsidence increases as the SST increases, or when the large-scale rising motion increases as the SST decreases. Figure 8a shows that these situations mainly occur over equatorial ocean regions, particularly over the warm pool region where the SST exceeds about 28°C (Fig. 9). At the seasonal timescale, the monsoon circulation associated with the thermal contrast between ocean and landmasses is a powerful source of modulation of the large-scale vertical motion that is independent on the local SST. The observed seasonal decoupling between the vertical motion and the SST may stem also from the remote influence of the intraseasonal variability on the regional monthly averaged vertical motion. Indeed, the spatial distribution of case II situations exhibits a maximum over the equatorial Indian Ocean and the western Pacific. This corresponds to regions where the convective activity is strongly affected by the Madden–Julian oscillation (Lau and Chan 1985; Weickmann et al. 1985; Madden and Julian 1994). Note that a maximum occurrence of case II is found for SSTs of about 29.5°C (Fig. 9). This is consistent with findings of Waliser (1996) that very high SSTs occur in regions of suppressed convection, in relation with the Madden–Julian oscillation.

c. El Niño/La Niña variations

For El Niño/La Niña variations, about 40% of monthly 1987–88 changes of the large-scale upward motion and SST fall into case I (Table 2). Figure 8b (top panel) shows that this occurs over most ocean regions at all latitudes, with a maximum over the central equatorial Pacific. Important exceptions are found, however, over the equatorial Indian Ocean and the western Pacific and, to a lesser extent, over the southern central Pacific eastward of New Guinea. In these regions, category II is dominant (Fig. 8b, central panel). As for seasonal variations, the occurrence of case II's reaches a maximum for SSTs of about 29.5°C (Fig. 9). These remote cases are related to the eastern shift of the main convergence zones over the equatorial tropical Pacific and to subsidence motions induced through mass continuity requirements by enhanced large-scale rising motions with SST. Case III's mostly occur over the eastern south-equatorial Pacific (Fig. 8b, bottom panel). In this region, large-scale vertical motion changes are weak with regard to SST changes.

5. Local relationships between SST, clouds, or radiation

a. Occurrence of the supergreenhouse effect

Raval and Ramanathan (1989) defined the greenhouse effect G by the difference between the surface LW emission and the outgoing LW radiation at the top of the atmosphere ($G = \sigma \mathrm{SST}^4 - \mathrm{LW}_{TOA}$). Ramanathan and Collins (1991) showed that over warm ocean regions (warmer than about 27°C), the increase of the greenhouse trapping with spatially increasing SST is faster than that of the surface emission (i.e., $dG/d\mathrm{SST} > 4\,\sigma \mathrm{SST}^3$) and found similar situations during the 1987 El Niño over the central and eastern Pacific Ocean. They referred to these situations as the supergreenhouse effect (SGE). These observations were subsequently confirmed by Hallberg and Inamdar (1993) examining seasonal variations in atmospheric greenhouse trapping and by Weaver et al. (1994) during the Central Equatorial Pacific Experiment (CEPEX).

An alternative and equivalent definition of the SGE is $dLW_{TOA}/d\mathrm{SST} < 0$. SGE situations thus occur whenever the outgoing LW flux decreases as the SST increases. The decrease of LW_{TOA} is due to the strong absorption and downward reemission of the surface emitted LW flux (Stephens et al. 1994) and to the absorption, by upper-tropospheric humidity and high-level clouds, of the LW radiation emitted by the surface and the lower troposphere and its reemission toward space at very cold temperatures. The temperature lapse rate also affects the LW emission of the atmosphere (Hallberg and Inamdar 1993; Bony and Duvel 1994; Inamdar and Ramanathan 1994), but this effect is comparatively weaker in the Tropics. Since high-level cirrus clouds and upper-tropospheric humidity are both closely related to the occurrence of convection, one may expect to find SGE situations in regions where the increase of the SST (and then of the surface LW emission) is as-

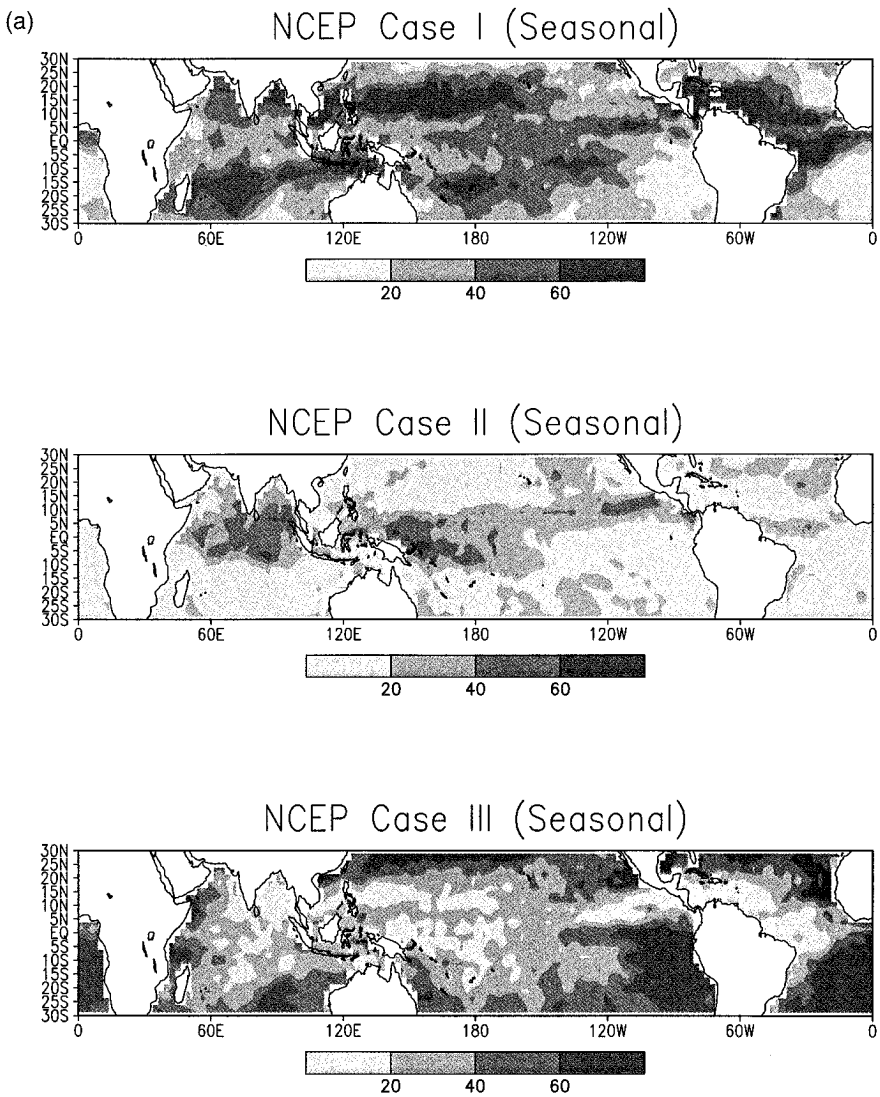

FIG. 8. Spatial distribution of the occurrence of the three cases defined in Table 2 for (a) seasonal variations and (b) El Niño/La Niña variations. Results are expressed as a percentage of the maximum possible occurrence (24 months for seasonal variations, 12 months for El Niño/La Niña variations).

sociated with enhanced convection. The occurrence of the SGE is thus likely to depend on the relationship between SST and large-scale vertical motion changes. We investigate below this dependence by analyzing the spatial distribution of the SGE inferred from seasonal and El Niño/La Niña variations of LW_{TOA} and SST over the tropical ocean.

The spatial distribution of the occurrence of $dLW_{TOA}/d\mathrm{SST} < 0$ situations derived from ERBE data for seasonal variations shows that SGE situations mostly occur around 10°–20°C of latitude, both in clear-sky and cloudy conditions (Fig. 10a). Consistently, this is where Gutzler and Wood (1990) and Raval et al. (1994) report the largest negative correlations between SST and LW_{TOA} variations. Note that as expected, the occurrence of clear-sky SGE situations over warm (convective) regions coincides with enhanced upper relative humidity (not shown). A weaker occurrence of SGE situations is found over subtropical ocean regions and over the equatorial tropical ocean, particularly over the Indian Ocean west of Sumatra and over the western Pacific. Expressed as a function of the SST, the occurrence of SGE situations is maximum for SSTs of about 27°C and decreases at warmer SSTs (Fig. 11a). These results are not specific to the 1987–88 period since they also appear in the 5-yr period 1985–89 (Figs. 10b and 11b). A new finding of this study is thus that on the seasonal timescale, SGE situations mostly occur on the edges of the warm pool area (for SSTs less than about 28°C) and decreases within the warm pool area (mainly over the tropical Indian Ocean and western Pacific), which is associated with warmer SSTs.

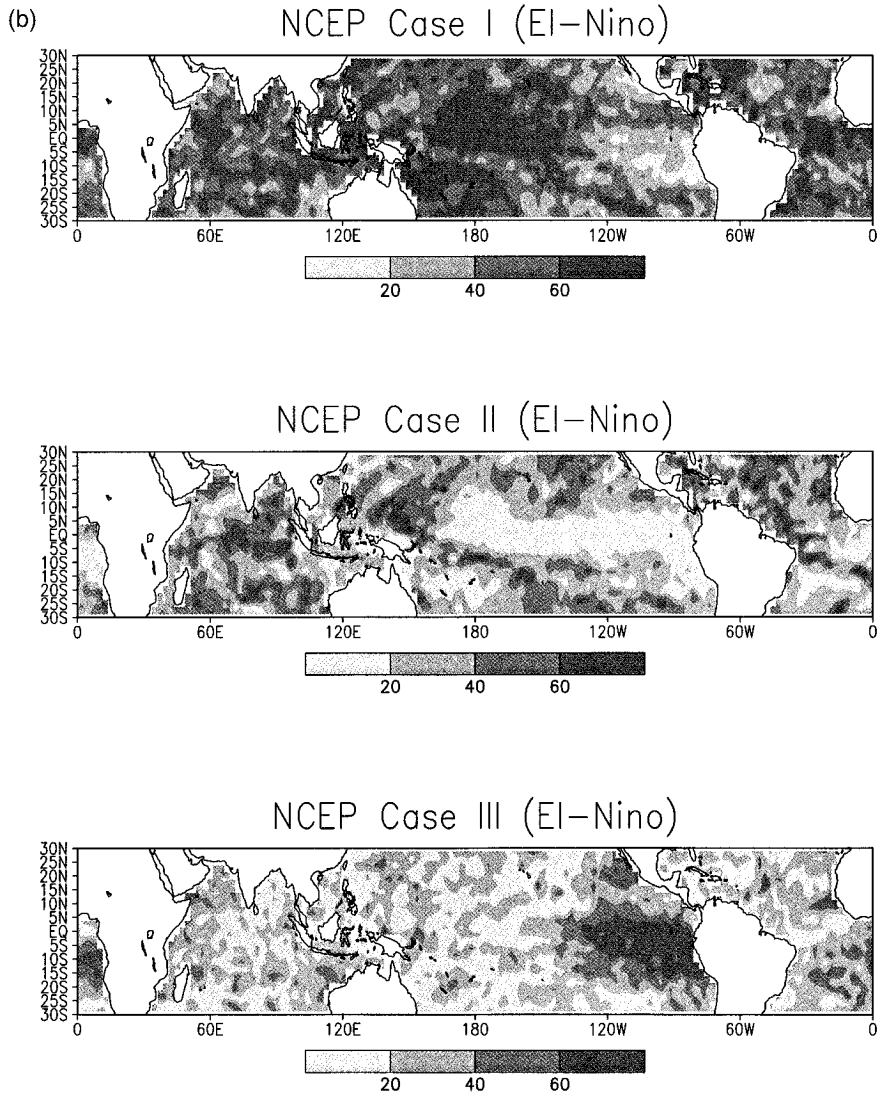

FIG. 8. (*Continued*)

The striking correspondence between Figs. 8a and 10a and between Figs. 8b and 12a shows that the seasonal occurrence of SGE situations is favored in regions where the ocean warming is associated with an enhanced large-scale rising motion (case I situations). As discussed in section 4b, this may occur through a combination of both thermodynamical and dynamical processes. Regions where the occurrence of SGE situations is weak mostly correspond to regions where case II situations are frequent—that is, over the warm pool regions for SSTs larger than 28°C and particularly for very high SSTs (Figs. 8a and 9a). This shows that SGE situations rarely occur in regions where the seasonal variability of the large-scale atmospheric vertical motion is decorrelated from local SST variations. This is particularly true over the equatorial regions of the eastern Indian Ocean and of the western Pacific Ocean, where remote processes associated with the internal intraseasonal variability of the atmosphere and the monsoon circulations contribute to this decorrelation.

Compared with seasonal variations, the SGE is more uniformly distributed spatially when considering El Niño/La Niña events of 1987–88 or monthly interannual variations during 1985–89 (Fig. 12). Nevertheless, a maximum of SGE occurrence is found over the equatorial central Pacific. This is where the ocean warming is maximum and where Ramanathan and Collins (1991) focused a large part of their study. This is consistent with the spatial distribution of case I situations during 1987–88 (Fig. 8b, top panel). ERBE data indicate that the SGE occurrence is weaker over the equatorial Indian Ocean and western Pacific during the 1987 El Niño, for SSTs warmer than about 28°–29°C (Fig. 13). Indeed, NCEP reanalyses indicate a larger occurrence of case II situations over these regions during this period (Figs. 8b and 9b). Over cold subtropical oceans, the occurrence

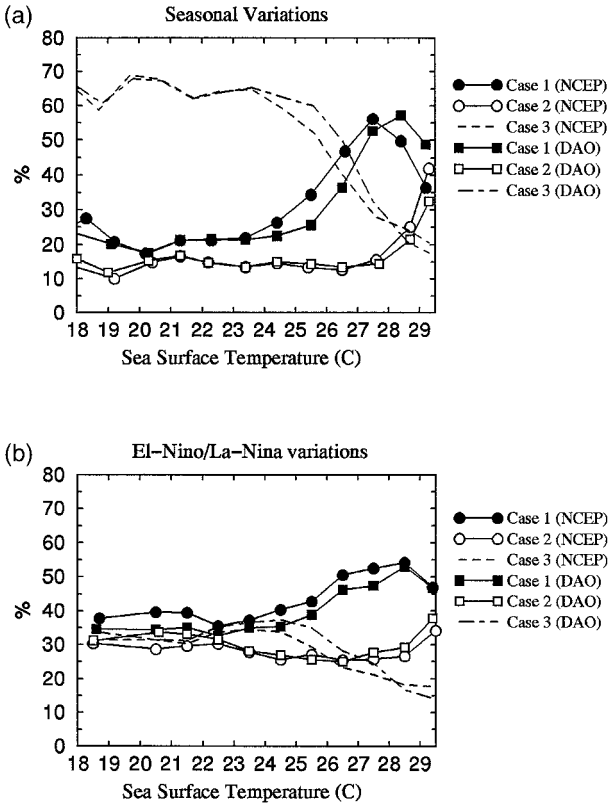

FIG. 9. Occurrence (expressed as a percentage of the total number of points within each SST interval of 1 K) of the different cases defined in Table 2 from NCEP and DAO reanalyses for (a) seasonal variations and (b) El Niño/La Niña variations.

of SGE situations is weaker, due to the persistence of large-scale subsidence (Fig. 8b, bottom panel), which prevents convection from occurring as the SST increases. Nevertheless, its average probability of occurrence reaches about 45% for SSTs of 23°–24°C (Fig. 13). This occurrence is larger than during seasonal variations (Fig. 11), which are associated with a smaller occurrence of case I situations over this range of SST (Fig. 9).

In conclusion, the analysis of seasonal and El Niño/La Niña changes in the SST and in the top of the atmosphere outgoing LW radiation shows that supergreenhouse effect situations occur whenever the regional ocean warming is associated with a large increase of the large-scale rising motion of the atmosphere. This occurs mostly on the edges of the warm pool area for SSTs less than about 28°C. On the other hand, their occurrence is reduced when large-scale vertical motion changes are decoupled from SST changes, due to remote or internal forcings of the atmospheric variability. This is the case in particular over the equatorial Indian Ocean and over the western equatorial Pacific, due to the monsoon circulations and the internal intraseasonal variability of the atmosphere.

b. Dependence of the cloud radiative forcing on SST

For a given SST change, the modification of the large-scale vertical motion may be highly variable according to the climate forcing and the timescale considered. During a seasonal cycle or an El Niño event, SST variations are very heterogeneously distributed over the tropical ocean and are often associated with profound variations of the large-scale circulation. The mean dependence of the cloud radiative forcing and other cloud parameters on SST that are inferred from spatiotemporal relationships (Fig. 2) are then largely influenced by the statistical relationship between the SST and the large-scale vertical motion (Figs. 3 and 4). However, weaker and longer-term variations of the tropical SST may be associated with much weaker changes of the large-scale circulation. In that case, the cloud–radiative feedbacks are likely to be more related to the thermodynamical effect of SST changes on cloud parameters than to large-scale dynamical influences.

By using a compositing procedure, we investigate below the sensitivity of the cloud radiative forcing to local SST changes for weak or no changes of the large-scale circulation (category III of SST/large-scale vertical motion relationships defined in Table 2). For seasonal or interannual variations, we compute a ''sensitivity index'' I_x (where x is a generic variable) defined as the linear regression coefficient of the least squares fit to $\Delta x = I_x\,\Delta\mathrm{SST}$; that is,

$$I_x = \frac{\sum (\Delta x\ \Delta\mathrm{SST})}{\sum (\Delta\mathrm{SST})^2}. \tag{1}$$

When considering seasonal variations, Δx is the difference between the monthly and annual mean values of x, and when considering El Niño/La Niña variations, it is the difference between the monthly mean values of x in 1987 and 1988 (Duvel and Bréon 1991; Bony et al. 1995). This coefficient is computed for different SST intervals of 1 K defined from the annual mean SST for seasonal variations, and from the 1988 monthly mean SST for El Niño variations. For each SST interval, we compute I_x by summing in Eq. (1) over all individual regions belonging to the SST interval under consideration. In parallel, a composite index $\tilde{I}_x$ is computed by restricting the sum to case III situations (Table 2). These situations are selected by using either NCEP or DAO reanalyses. The number of 2.5° × 2.5° regions considered to compute I_x and $\tilde{I}_x$ is reported in Figs. 13 and 14, respectively.

Here, I_x and $\tilde{I}_x$ are computed for the cloud radiative forcing and other cloud parameters on the basis of seasonal variations for the period 1987–88 (Fig. 15). Over cold ocean regions (SSTs less than about 25°–26°C), I_x and $\tilde{I}_x$ are quite similar. This is because these regions are associated with a persistent large-scale subsidence (Fig. 4), and the seasonal variations of the SST are mostly associated with no or weak variations of the large-scale vertical motion (Fig. 9a). As the SST in-

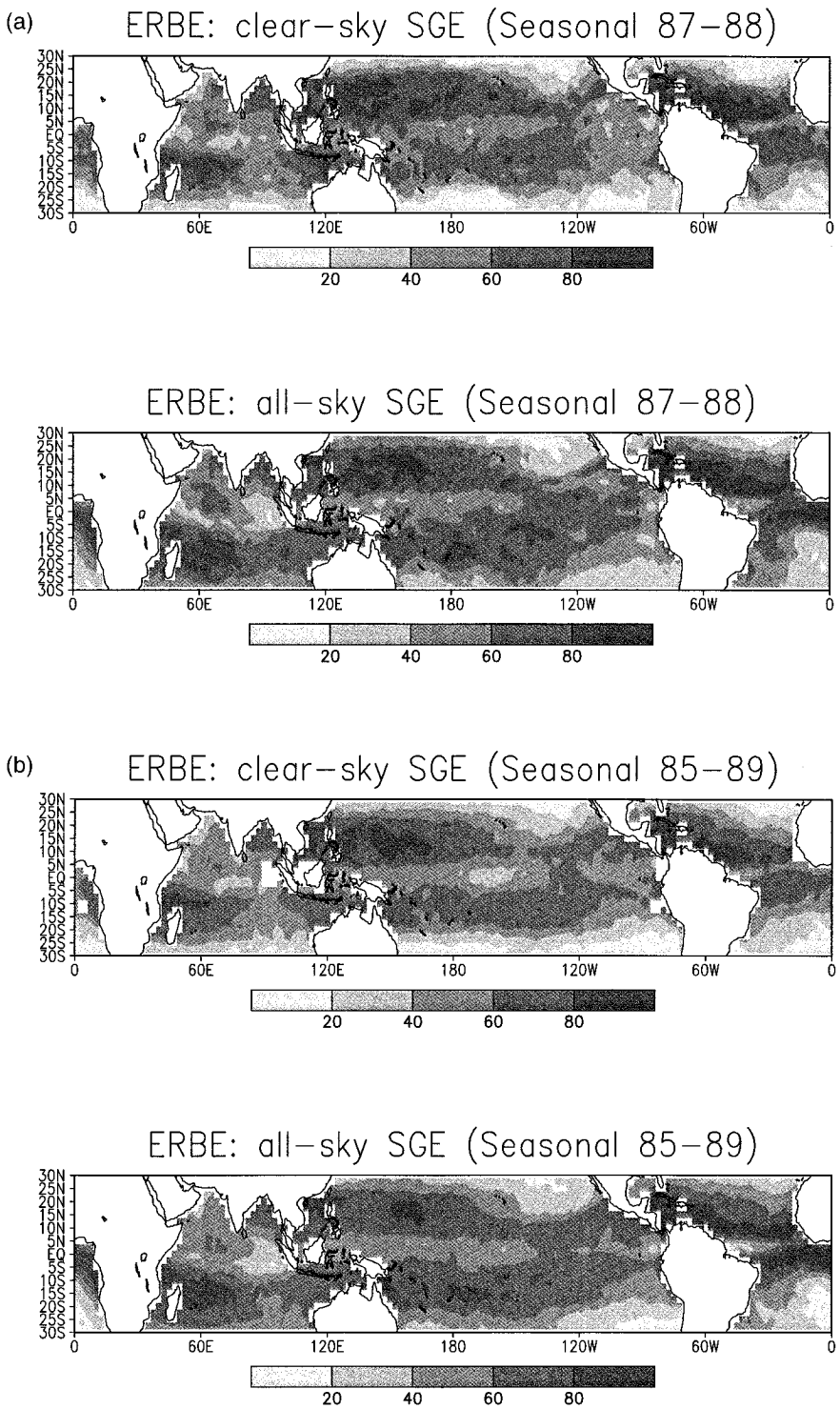

FIG. 10. Spatial distribution of the occurrence of supergreenhouse effect situations in (top) clear-sky and (bottom) all-sky conditions for seasonal variations during (a) 1987–88 and (b) 1985–89. The occurrence is expressed as a percentage of the maximum possible occurrence: (a) 24 months and (b) 60 months.

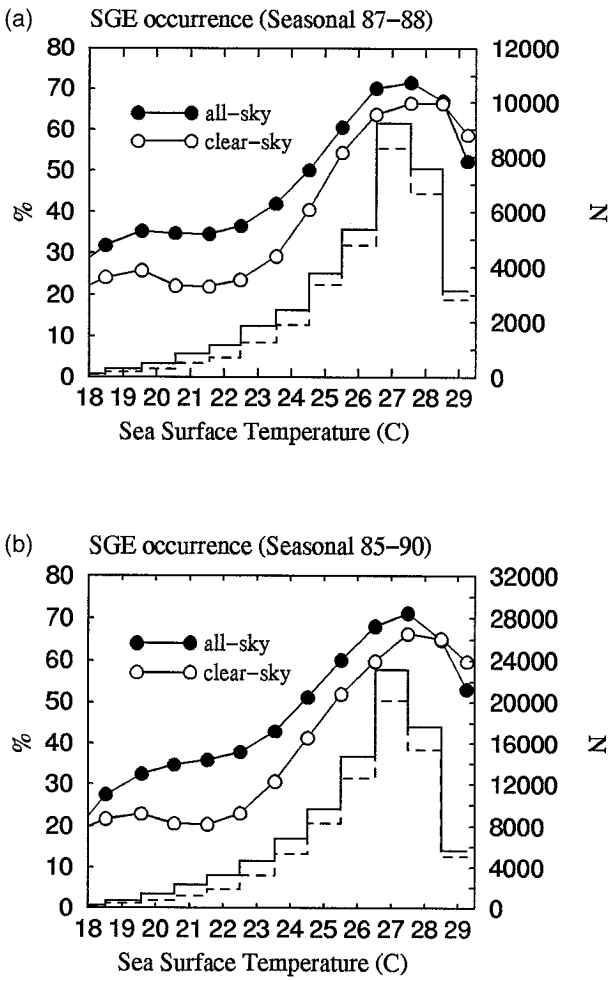

FIG. 11. Seasonal occurrence of supergreenhouse effect situations in clear-sky and all-sky conditions (white and black markers) as a function of the annual mean sea surface temperature for the periods (a) 1987–88 and (b) 1985–89. The occurrence is expressed as a percentage of the total number of points reported on the right side for all-sky conditions (plain line) and clear-sky conditions (dashed line).

creases, the SW component of the cloud radiative forcing decreases while the LW component remains constant. The sensitivity of C_{SW} is explained by the decrease of the cloud cover with SST (also inferred from Fig. 7) and by the decrease of the cloud optical thickness. Low-level clouds emit infrared radiation at a temperature that is close to that of the surface and of the low-level clear-sky atmosphere. They have thus a weak impact on the LW radiation at the top of the atmosphere, and their decrease with SST affects very little the LW cloud forcing.

Over warmer regions (SSTs larger than about 24°–25°C), case III situations represent only a weak fraction of the total number of situations (Fig. 9a), but $\tilde{I}_x$ is computed nevertheless from at least 3000 points (Fig. 14). In these regions, large discrepancies are found between I_x and $\tilde{I}_x$ (Fig. 15). The thermodynamical sensitivity of the SW cloud forcing and cloud fraction to local SST changes ($\tilde{I}_{C_{SW}}$ and $\tilde{I}_f$) represent only 20%–25% and 0%–20% of $I_{C_{SW}}$ and I_f, respectively. This shows that the seasonal changes of the cloud cover and of C_{SW} over warm ocean regions are intrinsically related to large-scale vertical motion changes, and that in the absence of large-scale vertical motion changes, they are weakly sensitive to local SST changes.

By comparison with C_{SW}, the thermal effect of SST changes on C_{LW} is larger: $\tilde{I}_{C_{LW}}$ is about 40%–50% of $I_{C_{LW}}$. Since the effective cloud cover remains roughly constant or decreases slightly with SST (Fig. 15f), C_{LW} changes are dominated by changes in the cloud-top temperature (Fig. 15d). Indeed, the sensitivity of the cloud-top pressure to local SST changes is reduced by only 30%–40% when large-scale dynamical effects are removed. The reason for the strong remaining thermal influence of the SST on the cloud-top pressure can be explained from simple thermodynamical arguments. The top of convective clouds occurs where the temperature of the cloud air parcel, which ascents along a moist adiabat, equals the temperature of the environmental air. When the SST increases, the cloud-base temperature changes to a new moist adiabat that crosses the environmental temperature profile at a higher altitude. In other words, the height of penetration of deep convection increases as the SST increases. This may explain the thermal effect of local SST changes on the observed cloud-top pressure and the C_{LW} despite the decrease of the cloud water path (Figs. 15b–d). Similar conclusions can be drawn when considering cloud and SST variations during El Niño/La Niña events (Fig. 16), which reinforce those inferred from the analysis of spatiotemporal relationships (Fig. 7).

Over cold ocean regions associated with low-level stratiform cloudiness, the SW component of the cloud radiative forcing dominates over the LW component (Figs. 15 and 16), and the seasonal or El Niño/La Niña changes of the C_{NET} with SST have the same sign as $dC_{SW}/d\mathrm{SST}$ (Fig. 17). This corresponds to a positive radiative feedback. Over warm ocean regions, there is a large compensation between LW and SW cloud forcing changes, but $dC_{NET}/d\mathrm{SST}$ is still slightly positive. This also constitutes a positive feedback. When SST changes are not associated with large-scale vertical motion changes (case III), the thermodynamical influence of SST on the detrainment height of deep convective clouds amplifies the LW cloud-forcing sensitivity. This leads to a weaker compensation between $dC_{LW}/d\mathrm{SST}$ and $dC_{SW}/d\mathrm{SST}$, and, therefore, $\tilde{I}_{C_{NET}}$ is slightly larger than $I_{C_{NET}}$ (Fig. 17). In the absence of large vertical motion changes (e.g., as for a uniform warming of the tropical ocean), $dC_{NET}/d\mathrm{SST}$ over tropical ocean is thus slightly more positive than that actually observed during seasonal or interannual variations.

6. Summary and discussion

Using NCEP and DAO meteorological reanalyses of sea surface temperature and large-scale atmospheric dy-

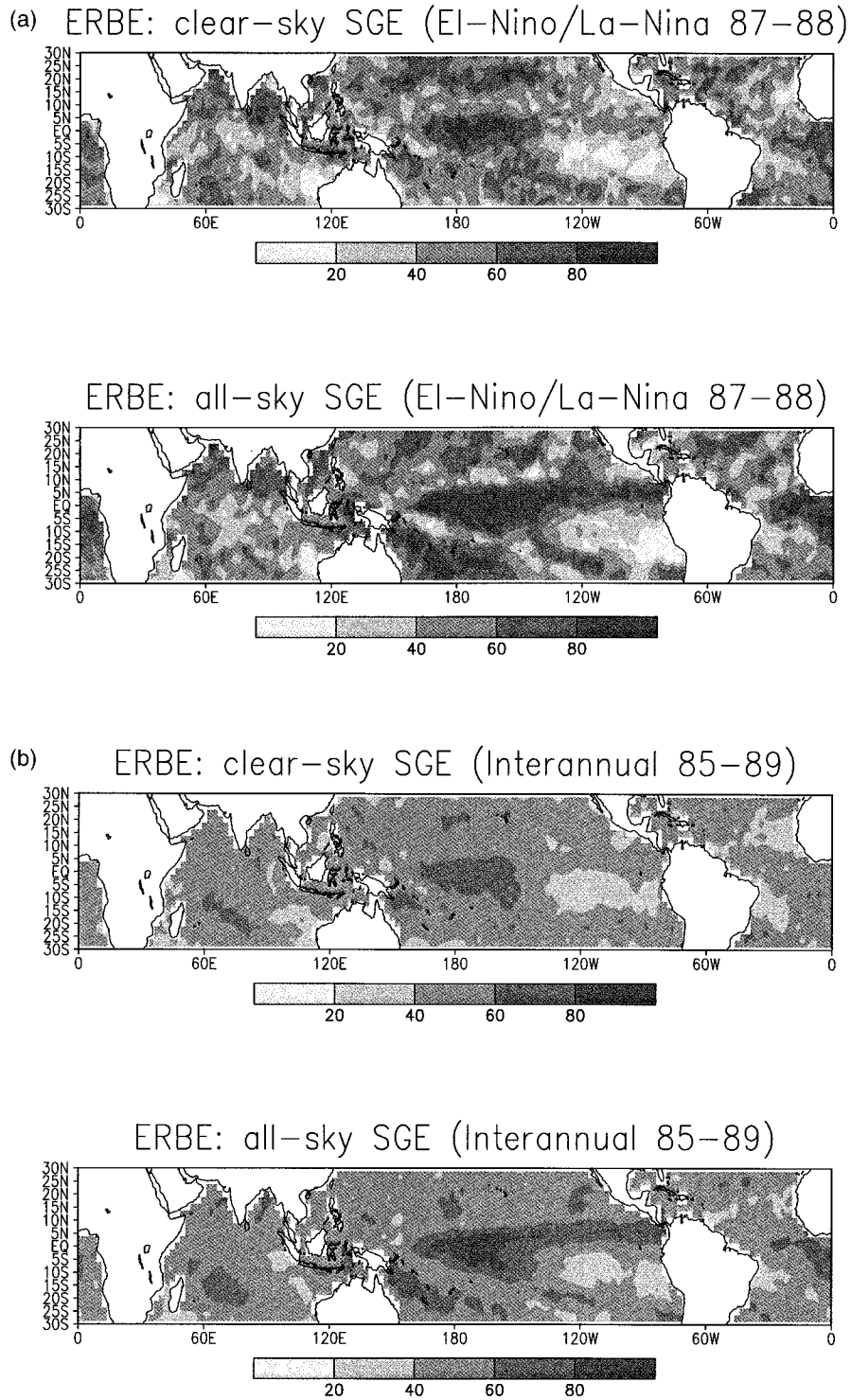

FIG. 12. Same as Fig. 10 except for (a) El Niño/La Niña variations during 1987–88 and (b) year-to-year monthly variations during 1985–89. The occurrence is expressed as a percentage of the maximum possible occurrence: (a) 12 months and (b) 120 months.

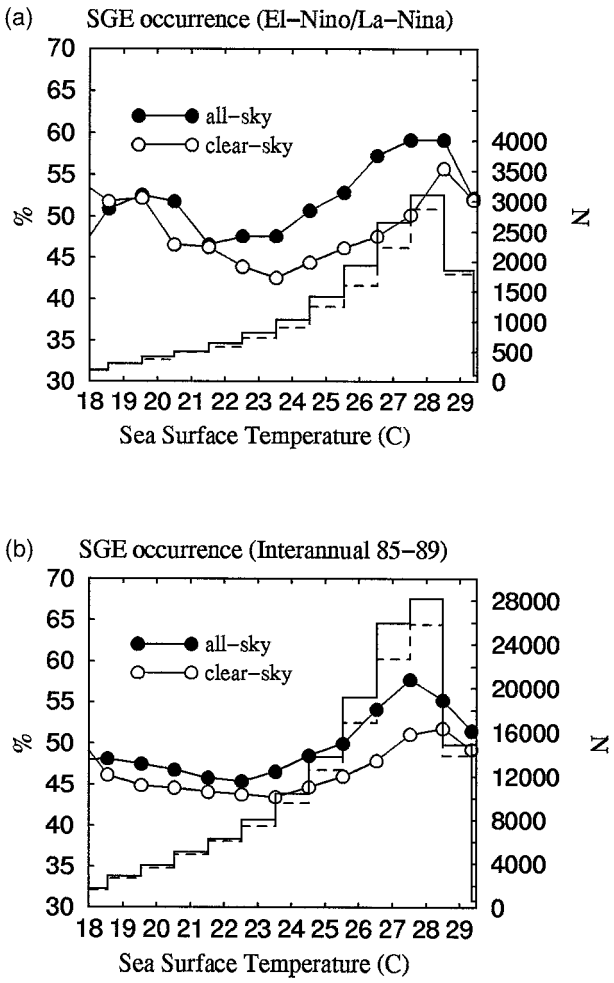

FIG. 13. Same as Fig. 11 except for (a) El Niño/La Niña variations during 1987–88 and (b) year-to-year monthly variations during 1985–89. The occurrence is expressed as a percentage of the total number of points reported on the right side for all-sky conditions (plain line) and clear-sky conditions (dashed line).

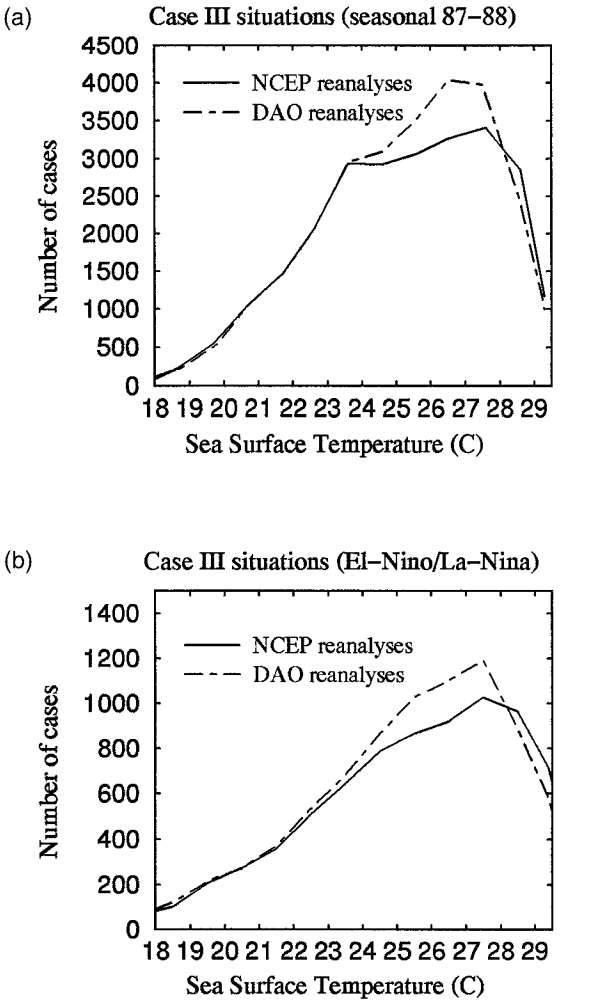

FIG. 14. Number of points from which the composite sensitivity index associated with case III situations is computed for (a) seasonal and (b) interannual variations.

namical fields for the period 1987–88 over tropical ocean (30°S–30°N), we have investigated the spatial, seasonal, and interannual relationships between the large-scale vertical motion of the atmosphere (described by the 500-hPa vertical velocity of the atmosphere at the resolution 2.5° × 2.5°) and the SST. Then, by using satellite data of water vapor, cloud, and radiation at the top of the atmosphere derived from independent datasets (ERBE, TOVS, ISCCP), we have investigated large-scale dynamical influences on the occurrence of super-greenhouse effect situations and on the dependence of the cloud radiative forcing on SST.

a. Relationships between the SST and the large-scale vertical motion of the atmosphere

It has been shown in several observational studies that the slope of the mean spatiotemporal relationships between the SST and water vapor and clouds or radiation is characterized by two discontinuities: one for SSTs of about 26°–27°C, and another around 29.5°C (Gadgil et al. 1984; Graham and Barnett 1987; Inoue 1990; Ramanathan and Collins 1991; Waliser et al. 1993; Zhang 1993). We show that these discontinuities are related to three different types of relationships between the large-scale atmospheric vertical motion and the SST. For SSTs less than about 26°–27°C, mostly (80%) large-scale subsiding motions are found over 2.5° × 2.5° ocean regions. Except for strongest subsidence motions located on the eastern part of cold subtropical ocean basins, the intensity of the large-scale subsidence is largely independent on the local SST. For SSTs warmer than about 26°–27.5°C, we note on the average a sharp increase with SST of both the frequency and the intensity of large-scale rising motions of the atmosphere. For SSTs warmer than about 29.5°C, strong rising motions still occur but the occurrence of weak subsiding motions

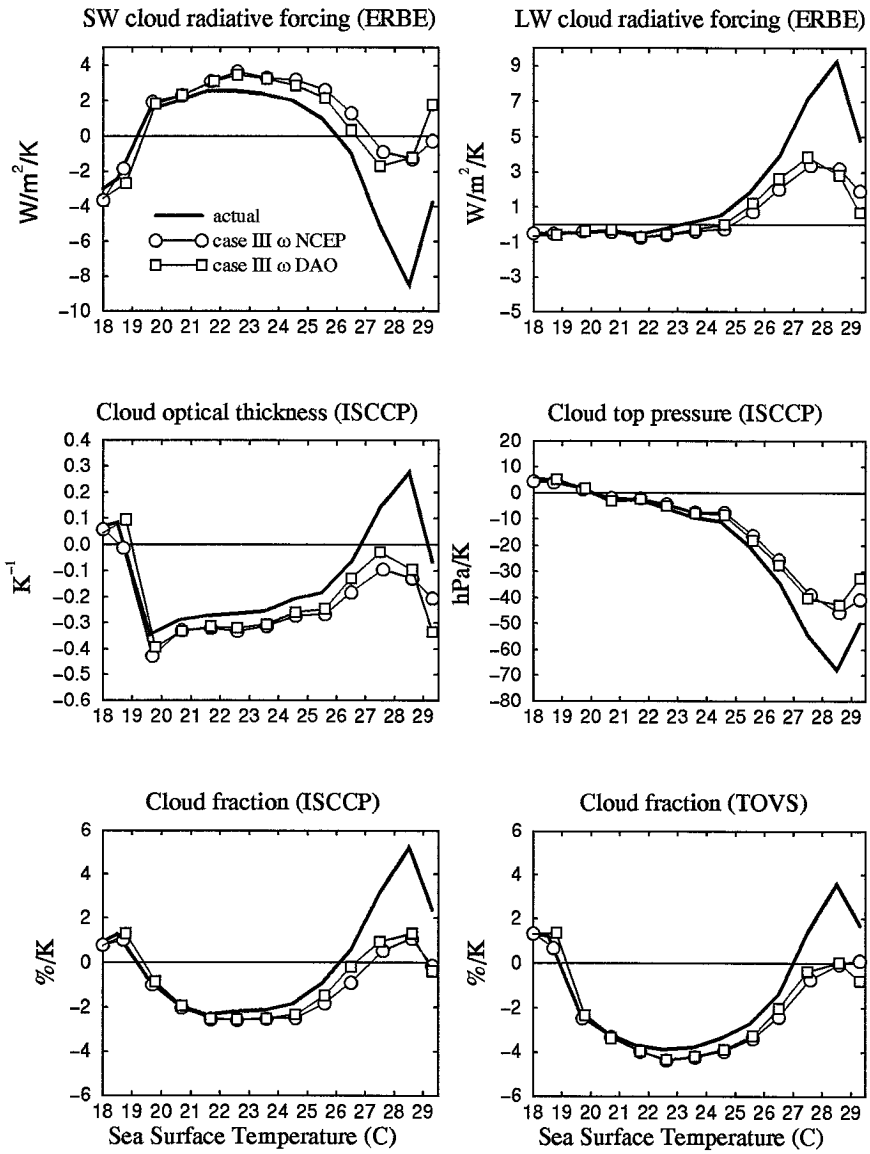

FIG. 15. Sensitivity index computed for the period 1987–88 on the basis of seasonal variations for the (a) SW cloud radiative forcing, (b) LW cloud radiative forcing, (c) cloud optical thickness, (d) cloud-top pressure, (e) cloud fraction derived from ISCCP data, and (f) cloud fraction derived from TOVS data. For each variable and each SST interval, an index is computed from the total number of points contained in the SST interval (referred to as actual). The composite case III indices are restricted to case III situations (as defined from NCEP or DAO reanalyses).

increases. Waliser and Graham (1993) explain this feature as follows: in regions of active convection, SST is limited to 29.5°C due to the shading effect of convective clouds; it is only when convection is suppressed by externally forced subsidence that the SST can exceed 29.5°C. This latter case should thus be interpreted as the forcing of the SST by the subsidence and not the other way around. The role of large-scale dynamical influences in the persistence of the two discontinuities at 26°–27°C and 29.5°C is confirmed by the almost disappearance of these discontinuities when considering individual large-scale circulation regimes (defined from the 500-hPa monthly mean vertical velocity).

The relationships between the SST and the large-scale vertical motion presented in this study are very consistent with those found in previous observational studies by using the outgoing LW radiation or highly reflective clouds as indices for tropical deep convection (Waliser et al. 1993; Zhang 1993). This shows that the occurrence of large-scale rising motions is intrinsically related to the occurrence of deep convection within the 2.5° × 2.5° area. This is consistent with the fact that in the

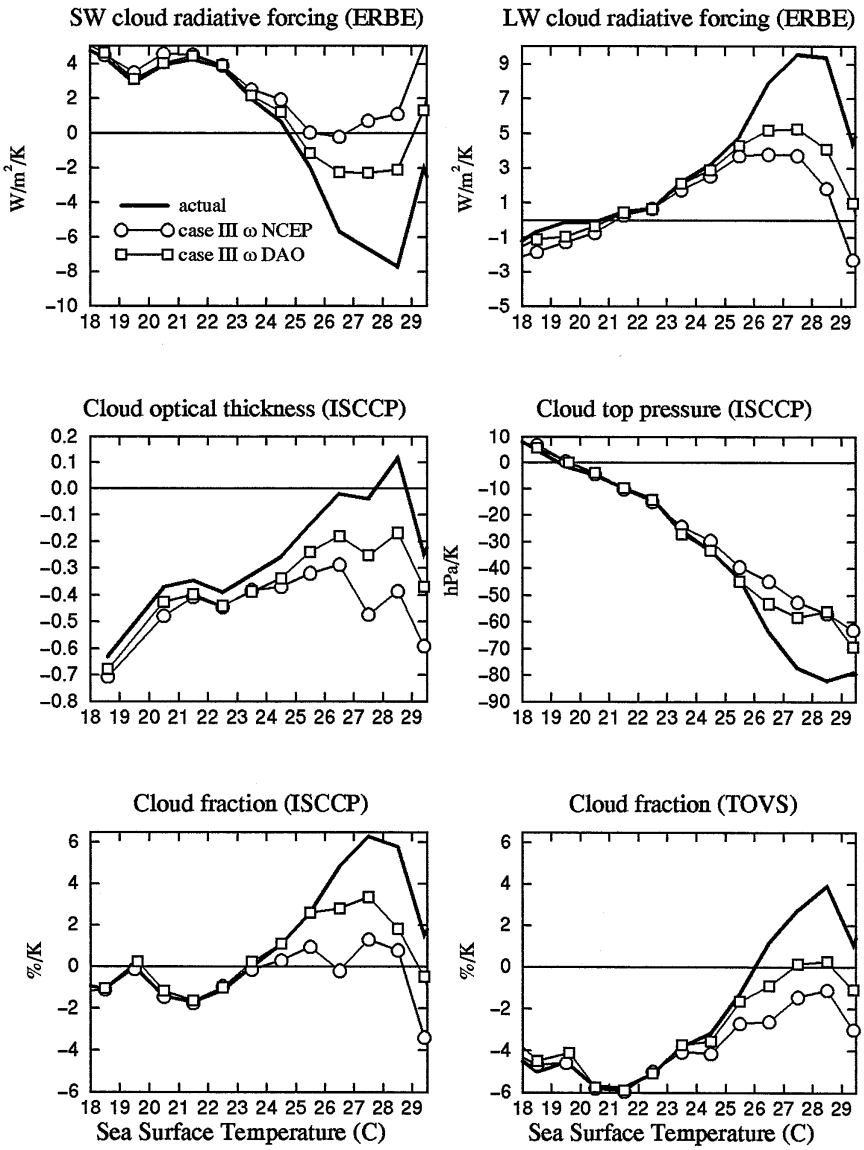

FIG. 16. Same as Fig. 15 except for El Niño/La Niña variations during 1987–88.

Tropics, and for a large range of timescales, moist convection is the primary mitigator of the adiabatic cooling produced by large-scale rising motion (Sud and Walker 1993).

b. Large-scale dynamical influences on the supergreenhouse effect

Ramanathan and Collins (1991) referred to situations where the increase of the greenhouse trapping with temperature is faster that of the surface emission as supergreenhouse effect (SGE). We examined the spatial distribution of the SGE occurrence by considering seasonal and interannual variations over the whole tropical ocean (including the western Pacific and the Indian Ocean) and investigated their dependence on the large-scale atmospheric circulation.

For both seasonal and interannual variations, we show that whatever the temperature of the surface ocean, the occurrence of SGE situations is intrinsically linked to the occurrence of enhanced large-scale atmospheric rising motion with increasing SST, which is itself intrinsically linked to the occurrence of deep convection. On the seasonal timescale, this occurs mostly around 10°–20° of latitude, in relation with the seasonal migration of the ascending and descending branches of the Hadley circulation. During an El Niño event, this occurs mostly over the equatorial central Pacific. On the other hand, the occurrence of SGE situations is weak in regions where the variability of the large-scale rising

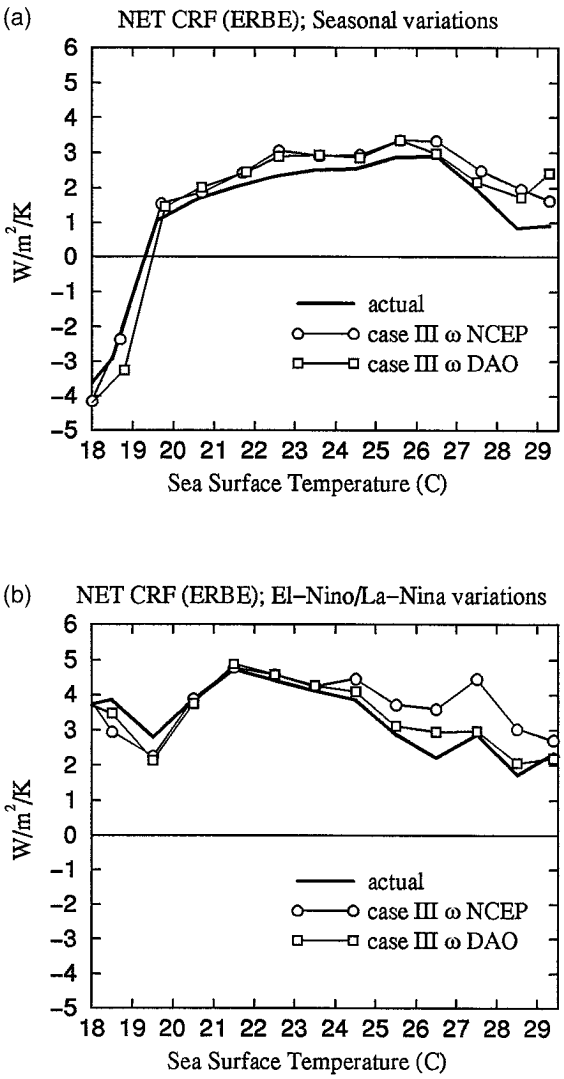

FIG. 17. Same as Fig. 15 and 16 except for the NET cloud radiative forcing for (a) seasonal variations and (b) El Niño/La Niña variations.

motion is largely decoupled (or decorrelated) from the local SST. When considering seasonal or El Niño/La Niña variations, these regions mostly occur over the warm pool area (for SSTs warmer than 28°C, and particularly for SSTs higher than 29.5°C), over the equatorial Indian Ocean and over the western equatorial Pacific. In these regions, indeed, the seasonal monsoon circulations and the intraseasonal variability of the atmosphere over the Indonesian region both constitute important sources of modulation of the large-scale vertical motion that are largely uncoupled to local SST variations. Over the equatorial Indian and western Pacific Oceans, the activation of feedback processes that regulate the sea surface temperature is thus likely to be more strongly related to the large-scale remote processes that govern the large-scale atmospheric circulation in this region than to the absolute value of the SST. Note, however, that this statement, which concerns warm regions of the equatorial Indian and western Pacific Oceans, may not hold for other regions of the tropical ocean.

c. Large-scale dynamical influences on the cloud radiative forcing

Considering either spatiotemporal, seasonal, or El Niño/La Niña variations, we find that whatever the range of SST considered, the cloudiness, the cloud optical thickness, and the SW cloud radiative forcing decrease with increasing SST in large-scale subsidence regimes. This confirms and extends previous observational results of Tselioudis et al. (1992), Oreopoulos and Davies (1993), and Norris and Leovy (1994) relative to cold subtropical ocean regions. The LW cloud forcing of low-level stratiform clouds being much weaker than the SW cloud forcing, the change of the net cloud forcing is strongly dominated by SW changes in these regimes.

Over warm oceans (SSTs warmer than 26°–27°C), both the LW and SW cloud forcing increase with increasing large-scale rising motion of the atmosphere. Nevertheless, the compensation between the LW and SW components is not complete and the net cloud radiative forcing increases slightly with SST (by 1 to 3 W m^{-2} K^{-1}). For a given value of the large-scale rising motion, the dependence of the SW cloud forcing on SST is weak. This shows that the large apparent sensitivity of the SW cloud forcing to SST changes deduced from the analysis of spatial, seasonal, or interannual variability, is mainly related to large-scale vertical motion changes that accompany SST changes (not necessarily through cause and effect relationships). In the absence of large-scale vertical motion changes, the rate of change of C_{SW} with SST is reduced to 20%–25% of its nominal value. By comparison, the reduction of the sensitivity of C_{LW} to SST changes is lesser. This is explained by the thermodynamical influence of the SST on the penetration height of deep convection and then on the cloud-top height. As a result, the increase of the net cloud forcing with SST is slightly more positive in the absence of large-scale vertical motion changes than in the presence of vertical motion changes. Since large-scale circulation changes mainly occur in association with modifications of the spatial distribution of SST (Lindzen and Nigam 1987), they are likely to be small in case of a uniform warming of the tropical ocean. With regard to the tropical radiation balance at the top of the atmosphere, the dependence of the cloud radiative forcing on SST may thus provide a positive climate feedback slightly larger in case of a uniform ocean warming than during seasonal or interannual variations.

Intercomparison experiments show that for a uniform ±2 K perturbation of the SST, the sign and the amplitude of the cloud radiative feedback produced by the different general circulation models are highly variable (Cess et al. 1989, 1990). The ability of the different models to

reproduce the LW and SW cloud-forcing sensitivities $\tilde{I}_{C_{LW}}$ and $\tilde{I}_{C_{SW}}$ of this study would certainly help to put strong constraints on the validity of the cloud–climate feedback simulated by these models. Also, the response of the greenhouse effect and the SW cloud radiative forcing to SST and large-scale circulation changes is known to be crucial for the simulation of climate by coupled ocean–atmosphere models (e.g., Meehl and Washington 1995). This study offers numerous diagnostic tools for assessing the coupling among the SST, the large-scale atmospheric circulation, the atmospheric hydrology, and the earth radiation budget in these models. Such stringent tests are required to improve current models and get confidence in the predictions of the earth's future climate.

Acknowledgments. The authors are grateful to Dr. Joel Susskind from NASA/GSFC for providing the TOVS Pathfinder Path A data, to Dr. Suranjana Saha from NCEP for her help in accessing NCEP reanalysis data, and to the Data Assimilation Office of the NASA/GSFC for providing DAO reanalysis data. Finally, the first author gratefully acknowledges Dr. Eugenia Kalnay for her encouragements and support during this study. Finally, the authors are grateful to Dr. V. Ramanathan and an anonymous referee for their thoughtful and useful comments. Part of this research was realized during the visit of the first author at the Climate and Radiation Branch of the NASA/Goddard Laboratory for Atmospheres, under the Universities Space Research Association (USRA) visitor program supported by the NASA Earth Observing System (EOS) ''Hydrologic Processes and Climate'' Interdisciplinary Investigation. Part of this study was supported by the French Electricité de France (EDF), by the Programme National d'Etude du Climat (PNEDC), and by the Environmental Program of the Commission of the European Communities.

REFERENCES

Albrecht, B. A., 1981: Parameterization of trade-cumulus cloud amounts. *J. Atmos. Sci.,* **38,** 97–105.

Barkstrom, B. R., 1984: The Earth Radiation Budget Experiment (ERBE). *Bull. Amer. Meteor. Soc.,* **65,** 1170–1185.

Betts, A. K., and W. Ridgway, 1989: Climatic equilibrium of the atmospheric convective boundary layer over a tropical ocean. *J. Atmos. Sci.,* **46,** 2621–2641.

Bony, S., and J.-P. Duvel, 1994: Influence of the vertical structure of the atmosphere on the seasonal variation of precipitable water and greenhouse effect. *J. Geophys. Res.,* **99,** 12 963–12 980.

——, ——, and H. Le Treut, 1995a: Observed dependence of the water vapor and clear-sky greenhouse effect on sea surface temperature: Comparison with climate warming experiments. *Climate Dyn.,* **11,** 307–320.

——, K.-M. Lau, and Y. C. Sud, 1995b: The super greenhouse effect and cloud radiative forcing in the tropical atmosphere. NASA Research and Tech. Rep., 200–202. [Available from NASA/GSFC, Greenbelt, MD 20771.]

——, Y. C. Sud, K.-M. Lau, J. Susskind, and S. Saha, 1997: Comparison and satellite assessment of NASA/DAO and NCEP/NCAR reanalyses over tropical ocean: Atmospheric hydrology and radiation. *J. Climate,* **10,** 1441–1462.

Cahalan, R., W. Ridgway, W. Wiscombe, and T. Bell, 1994: The albedo of fractal stratocumulus clouds. *J. Atmos. Sci.,* **51,** 2434–2455.

Cess, R. D., and Coauthors, 1989: Interpretation of cloud-climate feedback as produced by 14 atmospheric general circulation models. *Science,* **245,** 513–516.

——, and Coauthors, 1990: Intercomparison and interpretation of climate feedback processes in 19 atmospheric general circulation models. *J. Geophys. Res.,* **95,** 16 601–16 615.

Coakley, J. A., and D. G. Baldwin, 1984: Towards the objective analysis of clouds from imagery data. *J. Climate Appl. Meteor.,* **23,** 1065–1099.

Duvel, J.-P., and F. M. Bréon, 1991: The clear-sky greenhouse effect sensitivity to a sea surface temperature change. *J. Climate,* **4,** 1162–1169.

Emanuel, K., J. Neelin, and C. Bretherton, 1994: On large-scale circulations in convecting atmospheres. *Quart. J. Roy. Meteor. Soc.,* **120,** 1111–1143.

Fu, R., A. D. DelGenio, W. B. Rossow, and W. T. Liu, 1992: Cirrus-cloud thermostat for tropical sea surface temperatures tested using satellite data. *Nature,* **358,** 394–397.

——, ——, and ——, 1994: Influence of ocean surface conditions on atmospheric vertical thermodynamic structure and deep convection. *J. Climate,* **7,** 1092–1108.

——, W. T. Liu, and R. E. Dickinson, 1996: Response of tropical clouds to the interannual variation of sea surface temperature. *J. Climate,* **9,** 616–634.

Gadgil, S., P. V. Joseph, and N. V. Joshi, 1984: Ocean–atmosphere coupling over monsoon regions. *Nature,* **312,** 141–143.

Graham, N. E., and T. P. Barnett, 1987: Observations of sea surface temperature and convection over tropical oceans. *Science,* **238,** 657–659.

Gutzler, D., and T. Wood, 1990: Structure of large-scale convective anomalies over tropical oceans. *J. Climate,* **3,** 483–496.

Hallberg, R., and A. K. Inamdar, 1993: Observations of seasonal variations in atmospheric greenhouse trapping and its enhancement at high sea surface temperature. *J. Climate,* **6,** 920–930.

Hartmann, D. L., and M. L. Michelsen, 1993: Large-scale effects on the regulation of tropical sea surface temperature. *J. Climate,* **6,** 2049–2062.

Houghton, J. T., G. J. Jenkins, and J. J. Ephraums, Eds., 1990: *Climate Change: The IPCC Scientific Assessment.* Cambridge University Press, 365 pp.

Inamdar, A., and V. Ramanathan, 1994: Physics of greenhouse effect and convection in warm oceans. *J. Climate,* **7,** 715–731.

Inoue, T., 1990: The relationship of sea surface temperature and water vapor amount to convection over the western tropical pacific revealed from split-window measurements. *J. Meteor. Soc. Japan,* **68,** 589–606.

Kalnay, E., and Coauthors, 1996: The NCEP/NCAR 40-year reanalysis project. *Bull. Amer. Meteor. Soc.,* **77,** 437–471.

Klein, S. A., D. L. Hartmann, and J. R. Norris, 1995: On the relationships among low-cloud structure, sea surface temperature, and atmospheric circulation in the summertime northeast Pacific. *J. Climate,* **8,** 1140–1155.

Lau, K.-M., and P. Chan, 1985: Aspects of the 40–50 day oscillation during the northern winter as inferred from outgoing longwave radiation. *Mon. Wea. Rev.,* **113,** 1889–1909.

——, C. Sui, M. Chou, and W. Tau, 1994: An inquiry into the cirrus-thermostat effect for tropical sea surface temperature. *Geophys. Res. Lett.,* **21**(12), 1157–1160.

Lindzen, R. S., and S. Nigam, 1987: On the role of sea surface temperature gradients in forcing low-level winds and convergence in the tropics. *J. Atmos. Sci.,* **44,** 2418–2436.

Madden, R., and P. Julian, 1994: Observations of the 40–50-day tropical oscillation—A review. *Mon. Wea. Rev.,* **122,** 814–837.

Meehl, G., and W. Washington, 1995: Cloud albedo feedback and the super greenhouse effect in a global coupled GCM. *Climate Dyn.,* **11,** 399–411.

Meeson, B., F. Corprew, J. McManus, D. Myers, J. Closs, K.-J. Sun,

D. Sunday, and P. Sellers, 1995: ISLSCP Initiative I—Global Data Sets for Land–Atmosphere Models, 1987–1988. Vol. 5, NASA, CD-ROM. [Available from Goddard/EOSDIS/DAAC, Goddard Space Flight Center, Greenbelt, MD 20771.]

Norris, J. R., and C. B. Leovy, 1994: Interannual variability in stratiform cloudiness and sea surface temperature. *J. Climate,* **7,** 1915–1925.

Oreopoulos, L., and R. Davies, 1993: Statistical dependence of albedo and cloud cover on sea surface temperature for two tropical marine stratocumulus regions. *J. Climate,* **6,** 2434–2447.

Prabhakara, C., G. Dalu, R. C. Lo, and N. R. Nath, 1979: Remote sensing of seasonal distribution of precipitable water vapor over the oceans and the inference of boundary layer structure. *Mon. Wea. Rev.,* **107,** 1388–1401.

Ramanathan, V., and W. Collins, 1991: Thermodynamic regulation of ocean warming by cirrus clouds deduced from observations of the 1987 El-Niño. *Nature,* **351,** 27–32.

——, ——, and B. Subasilar, 1994: Comment on the paper ''An inquiry into the cirrus-cloud thermostat effect for tropical sea surface temperature.'' *Geophys. Res. Lett.,* **21**(12), 1185–1186.

Raval, A., and V. Ramanathan, 1989: Observational determination of the greenhouse effect. *Nature,* **342,** 758–761.

——, V. Oort, and H. Ramaswamy, 1994: Observed dependence of outgoing longwave radiation on sea surface temperature and moisture. *J. Climate,* **7,** 807–821.

Reynolds, R. W., and T. M. Smith, 1994: Improved global sea surface temperature analyses. *J. Climate,* **7,** 929–948.

Rossow, W., and R. Schiffer, 1991: ISCCP cloud data products. *Bull. Amer. Meteor. Soc.,* **72,** 2–20.

——, L. C. Garder, P. J. Lu, and A. Walker, 1991: International Satellite Cloud Climatology Project (ISCCP) documentation of cloud data. WMO/TD No. 266, 76 pp. plus 3 appendixes. [Available from World Meteorological Organization, Case Postale 2300, CH-111 Geneva 2, Switzerland.]

Schubert, S. D., J. Pfaendtner, and R. Rood, 1993: An assimilated dataset for earth science applications. *Bull. Amer. Meteor. Soc.,* **74,** 2331–2342.

Sellers, P., and Coauthors, 1995: An Overview of the ISLSCP Initiative I—Global Data Sets. ISLSCP Initiative I Global Data Sets for Land–Atmosphere Models, 1987–1988. Vol. 1, NASA, CD-ROM. [Available from Goddard/EOSDIS/DAAC, Goddard Space Flight Center, Greenbelt, MD 20771.]

Stephens, G. L., 1990: On the relationship between water vapor over the oceans and sea surface temperature. *J. Climate,* **3,** 634–645.

——, and T. J. Greenwald, 1991a: The Earth's radiation budget and its relation to atmospheric hydrology, 1. Observations of the clear-sky greenhouse effect. *J. Geophys. Res.,* **96,** 15 311–15 324.

——, and ——, 1991b: The Earth's radiation budget and its relation to atmospheric hydrology, 2. Observations of cloud effects. *J. Geophys. Res.,* **96,** 15 325–15 340.

——, A. Slingo, M. J. Webb, P. J. Minnett, P. H. Daum, L. Kleinman, I. Wittmeyer, and D. A. Randall, 1994: Observations of the Earth's radiation budget in relation to atmospheric hydrology, 4. Atmospheric column radiative cooling over the world's oceans. *J. Geophys. Res.,* **99,** 18 585–18 604.

Sud, Y. C., and G. K. Walker, 1993: A rain evaporation and downdraft parameterization to complement a cumulus updraft scheme and its evaluation using GATE data. *Mon. Wea. Rev.,* **121,** 3019–3039.

Susskind, J., P. Piraino, L. Rokke, L. Iredell, and A. Mehta, 1997: Characteristics of TOVS Pathfinder Path A dataset. *Bull. Amer. Meteor. Soc.,* **78,** 1449–1472.

Tselioudis, G., W. Rossow, and D. Rind, 1992: Global patterns of cloud optical thickness variation with temperature. *J. Climate,* **5,** 1484–1495.

Waliser, D. E., 1996: Formation and limiting mechanisms for very high sea surface temperature: Linking the dynamics and the thermodynamics. *J. Climate,* **9,** 161–188.

———, and N. E. Graham, 1993: Convective cloud systems and warm-pool SSTs: Coupled interactions and self-regulation. *J. Geophys. Res.,* **98,** 12 881–12 893.

——, ——, and C. Gautier, 1993: Comparison of the highly reflective cloud and outgoing longwave radiation datasets for use in estimating tropical deep convection. *J. Climate,* **6,** 331–353.

Weaver, C., W. Collins, and H. Grassl, 1994: Relationships between clear-sky atmospheric greenhouse effect and deep convection during the Central Equatorial Pacific Experiment: Model calculations and satellite observations. *J. Geophys. Res.,* **99,** 25 891–25 901.

Weickmann, K., G. Lussky, and J. Kutzbach, 1985: Intraseasonal (30–60 day) fluctuations of outgoing longwave radiation and 250 mb streamfunction during northern winter. *Mon. Wea. Rev.,* **113,** 941–961.

Zhang, C., 1993: Large-scale variability of atmospheric deep convection in relation to sea surface temperature in the tropics. *J. Climate,* **6,** 1898–1913.